THE RELATIONSHIP BETWEEN MICROSTRUCTURE AND MECHANICAL BEHAVIOR IN BETA TITANIUM-VANADIUM ALLOYS

A THESIS

Presented to

The Faculty of the Division of Graduate Studies

by

Henry Grady Paris

In Partial Fulfillment

of the Requirements for the Degree

Doctor of Philosophy in the School of Chemical Engineering

Georgia Institute of Technology

August 1975

THE RELATIONSHIP BETWEEN MICROSTRUCTURE AND MECHANICAL BEHAVIOR

IN BETA TITANIUM-VANADIUM ALLOYS

Approved:

Bruce G. Lefevre, Chairman

Edgar A. Starke Jr.

David Kalish

Date approved by Chairman: 9/18/75

ERRATUM

Page number 10 does not appear in this dissertation. This does not constitute a missing page but an error in pagination.

ACKNOWLEDGMENTS

Several contributions to this work must be acknowledged. The helpful discussions of technical and experimental points with Drs. S.B. Chakrabortty, D. Kalish, B G. Lefevre, T.H.B. Sanders, E.A. Starke Jr., J.C. Williams, and Mr. John Rinker were essential to this work. The cooperation and experience of Mr. Charles Blackwood of the Chemical Engineering Machine Shop is gratefully acknowledged. The most important distribution to be acknowledged is that of my parents, Doris Kennedy Paris and Grady Vaughan Paris, who nutured my desire to learn by ceaseless encouragement to seek explanation of that which is not understood and never to lose an abhorrence of the tyranny of ignorance and intolerance. This research was made possible by the financial support of the Office of Naval Research, Contract N00014-75-C-0349, NR 031-750.

TABLE OF CONTENTS

TABLE OF CONTENTS (Continued)

LIST OF TABLES

LIST OF ILLUSTRATIONS

LIST OF ILLUSTRATIONS (Continued)

LIST OF ILLUSTRATIONS (Continued)

SUMMARY

Titanium alloys containing 20, 24, 28, and 32% vanadium by weight are observed to deform primarily by coarse $\{\overline{1}12\}\langle 111\rangle$ twinning when containing moderate volume fractions of the omega phase ($\lesssim 0.6$). These alloys possess good ductility relative to alloys containing greater volume fractions of the omega phase. Deformation in the latter alloys is characterized by predominant planar slip which results in embrittlement. The unusual ductility of the alloys which deform predominantly by twinning is explained by the homogeneity of the twinning deformation on a microscopic level. The coarse twin products are observed to be established by repeated layering of microtwin bands of the same mode. Regardless of the fact that the direct atomic motions in $\{\overline{1}12\}\langle 111\rangle$ twinning do not preserve the omega structure, $\{\overline{1}12\}\langle 111\rangle$ deformation twins in alloy compositions of less than or equal to 24% V contain the omega phase in the proper orientations relative to the cubic twinned lattice. The compatibility of the twinning deformation with certain orientations of the omega phase is noted and a mechanism is offered which explains: (i) how a $\{\overline{1}12\}\langle 111\rangle$ twin nucleus may be created at an omega/beta interface, and (ii) how a twin shear may be accommodated within the coherent omega precipitate by dilation or temporary reversion of the omega structure. The consequence of the dilation is a subsequent athermal transformation to either the BCC twinned structure or the omega structure. The ductility of certain alloys is explained in terms of the relative volume of BCC material per omega particle available for effecting a macroscopic

deformation mechanism involving both phases.

CHAPTER I

INTRODUCTION

The class of body-centered cubic titanium beta isomorphous alloys possess similar phase relations. One distinguishing feature of these alloys is the occurrence of the metastable hexagonal omega phase which possesses similar structure and particle morphology for a number of solute additions (1). A commercial alloy of this type is called Beta III, whose binary prototypes are Ti-Mo alloys containing less than 11% Mo. Other Ti-V beta isomorphous alloys are the subject of this study. The deformation characteristics of these beta isomorphous alloys have not been commercially exploited because omega phase strengthening is not well understood or easily accomplished. The deformation character and its dependence on the omega phase in Ti-V alloys bear certain similarity to Beta III alloy behavior.

Marked changes in mechanical properties and deformation behavior are observed with variation in solute content in quenched and deformed beta Ti-V alloys (4,62). Twinning is observed to be a major deformation mode below about 36% vanadium content. The twin fault probability has been determined to vary with composition in a manner unexpected in BCC solid solutions. The occurrence of a coarse twin product at low compositions is thought to be associated with the occurrence of the omega phase. Much information remains to be determined on the specific influence of the omega phase on deformation in these alloys.

Though much experimental work has been done involving deformation twinning, many fundamental questions remain unanswered (5-10). Mechanisms are seldom proposed to explain more complex twinning than the classically encountered $\{\overline{1}12\}\langle 111\rangle$ mode in BCC metals and alloys. Even less is known of the effect of metallurgical variables on twinning in multiphase alloys. The effects of precipitation parameters such as particle size, misfit and volume fraction remain largely unexplored. It is the purpose of this study to ascertain the influence of solute content on the deformation behavior of beta Ti-V alloys. The influence of the omega phase on deformation is investigated. Compatibility of the twinning deformation to the omega structure is examined and possible mechanisms accounting for the twinning are discussed.

CHAPTER II

THE LITERATURE

Titanium-Vanadium Phase Relations

In solute lean Ti-V alloys, the high temperature beta phase may be retained partially or totally upon quenching depending upon the solute content (1). This part of the phase diagram (Figure 1) may be divided into three regions according to the phase transformation which occurs upon quenching and/or aging (11). In alloys containing up to 10-12% vanadium (well into the HCP alpha plus BCC beta region) martensitic alpha prime occurs upon quenching. At higher solute contents to about 24% vanadium, a metastable hexagonal phase, omega, athermally forms upon quenching. The athermal transformation cannot be suppressed even with extremely rapid quenching. The exact value of solute content necessary to suppress the athermal transformation depends on impurity content and sample configuration. The temperature, T_c, below which omega forms depends on interstitial content and solute identity (12-15). In a study of Ti-17% V, 1000 ppm (wt.) oxygen content supressed the omega transformation (16,17). The reversibility of the athermal transformation has been established (18). At higher solute contents ($\lesssim$ 40%V) there is some dispute as to the exact nature of the phase relations. Though the omega phase occurs rapidly since it is a diffusion independent process, it does not necessarily occur spontaneously (37). Some investigators have reported the presence of a decomposition of the beta structure into

solute lean and solute rich portions, while others have reported the presence of omega upon aging (1,4).

The omega phase is a coherently precipitated product possessing a well defined crystallographic relationship to the parent BCC beta lattice:

$$\langle 1\bar{1}0\rangle_{\beta} \;//\; \langle 11\bar{2}0\rangle_{\omega} \quad \text{and} \quad \{111\}_{\beta} \;//\; \{0001\}_{\omega} \; .$$

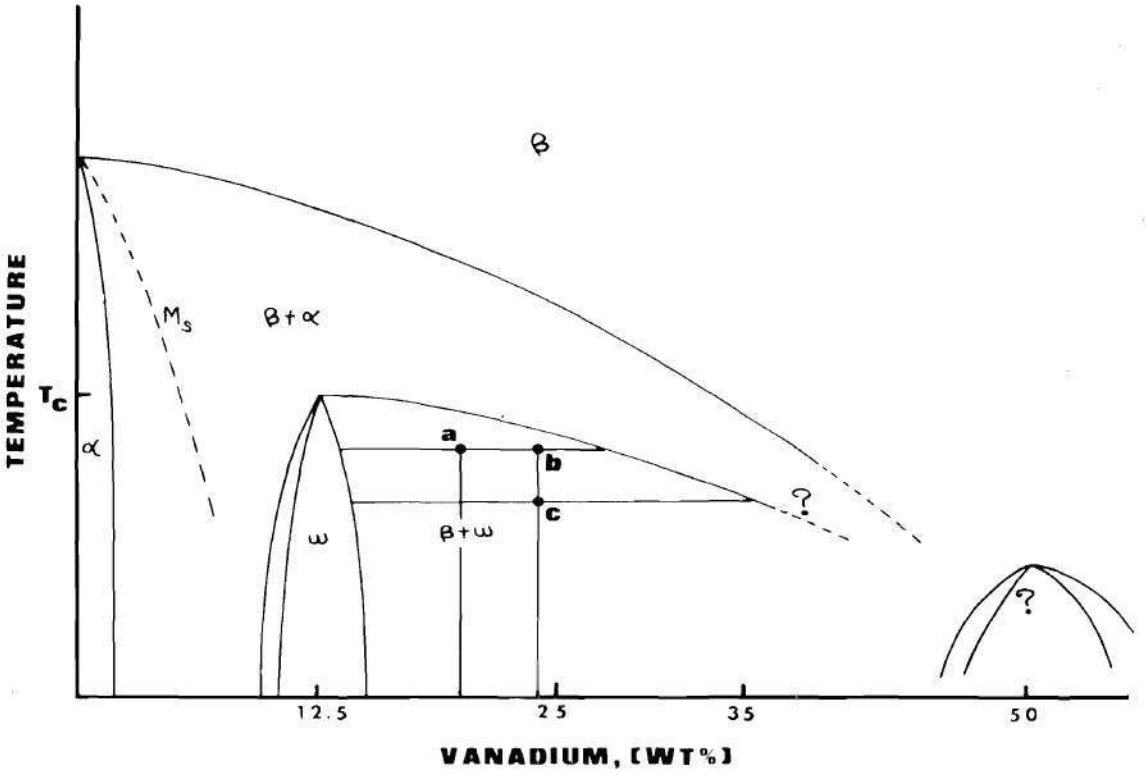

Figure 1. The Titanium - Vanadium Phase Diagram

Silcock and Bagariatskii respectively refer to the omega crystallographic structure as hexagonal and trigonal (19,20). Sass and Borie show that

a transition in structure from trigonal to hexagonal occurs with decreasing solute content (3). The problems encountered in using the hexagonal notation for planes and directions in the omega phase are discussed in Appendix I. The four orientation variants and specific crystallographic relationships between the beta and omega lattices are presented in Appendix II.

The omega particle morphology depends on the coherency strain associated with the transformation. This is a solute dependent parameter (1). In alloys whose misfit strain is less than 1%, e.g., Ti-Mo, Ti-Nb, and Ti-Ta, ellipsoidal particles whose major axis is up to 1000 Å long occur, while in those alloys whose misfit exceeds this value, e.g., Ti-V, Ti-Ni, and Ti-Cr, cuboidal precipitates of edge length up to 500 Å occur.

Hickman has determined the variation of several precipitation parameters with aging time, solute content and aging temperature in Ti-V alloys (12,14,21). Over the limited compositional range where omega forms athermally, no compositional changes occur upon the transformation. This is a result of the diffusion independent nature of the transformation. It implies only minimal misfit exists during the early stages of precipitation. Alloys of increased solute content transform in a similar manner upon aging. In both situations compositional adjustments occur at a constant volume fraction after precipitation has ended. The omega rejects solute, enriching the matrix and increasing the particle/matrix misfit.

It has been suggested that the misfit determines the stability of the omega phase. This suggestion is based on the hypothesis that many intermediate coherent phases owe their stability to the constraint of the parent lattice. After prolonged aging, dislocations are observed in

the matrix/particle interface. The stable alpha phase is observed to nucleate on these misfit dislocations and to consume the omega phase prior to the decomposition of the beta lattice (22).

The beta to omega transformation has been described by several models (24,53,18). A mechanism of {111} plane collapse accurately describes the atomic motions required to create the structure but does not adequately explain the diffuse intensity observed via x-ray and electron diffraction experiments. The actual transformation appears to involve correlated displacement of rows of atoms by $\pm 1/12$ <111>, equivalent to shuffling of $\{\overline{1}\overline{1}2\}$ planes by the same amount. The $\{\overline{1}\overline{1}2\}$ shuffle model of the transformation predicts several athermal embryonic morphologies. Among these are: (i) discs lying either singularly or in groups of three on the $\{\overline{1}\overline{1}2\}$ planes containing the same <111> direction, or (ii) rods of omega parallel to the <111> direction that is the omega orientation variant's $\bar{c}$ axis.

The martensitic alpha prime transformation has been previously suggested to occur by similar $\{\overline{1}\overline{1}2\}$ shuffles (23,25). The shuffles in this situation are in the same direction but like the $\{\overline{1}\overline{1}2\}$ <111> twinning transformation shuffles (56), are twice the magnitude of those required to produce the omega structure. The omega transformation is illustrated in Figure 2a. The similarity of the omega and alpha prime transformations to the phenomenon known as "shuffle twinning", illustrated in Figure 2b, suggest that both are intimately related to the $\{\overline{1}\overline{1}2\}$ <111> twinning transformation.

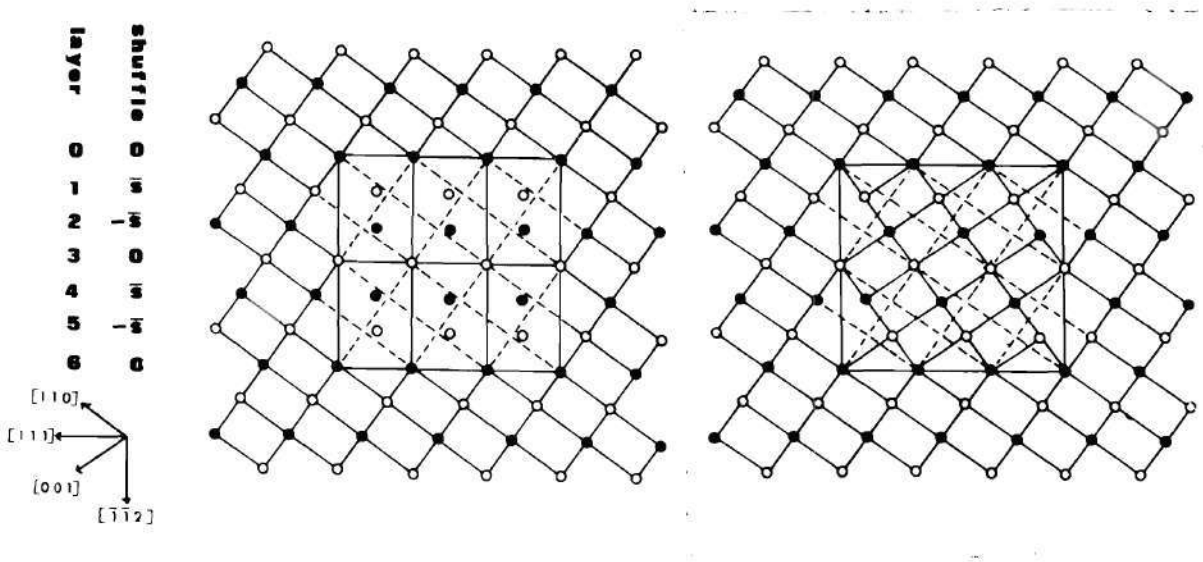

(a) (b)

Figure 2. An Illustration of the <111> Atom Shuffles in the Omega and $\{\bar{1}\bar{1}2\}$ <111> Shuffle Twin Transformations. (a) The omega atom shuffles, $\bar{S} = \pm 1/12$ <111>. (b) The $\{\bar{1}\bar{1}2\}$ <111> twin atom shuffles, $\bar{S} = \pm 1/6$ <111>.

Mechanical Properties and Deformation Behavior of Quenched Ti-V Alloys

The mechanical behavior of unaged beta Ti-V alloys between the compositional limits of 20-40%V varies markedly (4). In the lower solute range of this interval, a coarse deformation twin product is observed. The mode has been identified as $\{\bar{1}\bar{1}2\}$ <111> twinning. The lower solute alloys have good ductility. At higher solute contents, the twinning occurs on a much finer scale and is accompanied by predominant slip and less ductility. Increased twinning is again noted at 40% V. Athermal omega is reported in alloys up to 24% V.

Deformation Twinning

Deformation twinning has been the subject of numerous investigations in past years (5-10). The references cited provide an excellent treat-

ment of the crystallographic and physical nature of the subject and provide a thorough review of the subject. Basically slip and twinning are the fundamental modes of plasticity. Slip involves atomic motion on glide planes of magnitude equal to the nearest neighbor distance on glide planes. Twinning can be imagined to occur by shearing on twin planes of magnitude equal to only a fraction of the nearest neighbor distance. Twinning and slip are interrelated. It is believed a certain amount of slip is necessary for twin nucleation (38-40). Twinning provides an alternative deformation mode when slip is inhibited.

A twin is defined as "a region in a crystalline body that has undergone a homogeneous shape change in such a way that the product structure is identical to the parent save for orientation differences" (26). Subsequent investigators define a twin shear as a "shear which restores the lattice to a new orientation" (27,28).

Formal theories of the crystallography of the twinning transformations have been developed (5,6,9,10,26-29). Four crystallographic parameters, along with the shear, characterize a twin completely. Of these four parameters, two are planes which remain undistorted after twinning; one, K_1, remaining unrotated while the other, K_2, is rotated $180^\circ - 2\phi$ about an axis perpendicular to the plane. 2ϕ is the final angle between K_1 and K_2. The third and fourth elements are η_1, the shear direction and η_2, the direction defined by the intersection of the shear plane and K_1. Either η_1 and K_2, or η_2 and K_1 define the other two parameters.

The occurrence of specific twinning modes has been explained in terms of minimal atomic shears and d-spacings of twinning planes (30,31,38-40). Later work has generalized the twinning theory accounting for various twin

modes on the basis of the above criteria and the nature and magnitude of atomic shuffles which may be involved in the twinning mode (26-28,32). The latter treatment accounts for all known twinning modes and predicts others not yet experimentally verified. It is concluded that to account for all the modes predicted by a theory, a convenient dislocation mechanism must be available to account for the required atomic motions (32). This assumption has been made by several investigators, at least implicitly, (46-51); however, a recent treatment of the martensitic transformation (which bears certain similar similarities to the twinning transformation) suggests specific dislocation models are not necessary to explain the transformations (57).

The nature of the solute, as well as the morphology of any second phases affects the twinning behavior of alloys. Interstitial additions are observed to inhibit twinning because an interstitial atom cannot be translated to an equivalent site by the twin shear. Substitutional additions are suggested to enhance twinning by such factors as raising the yield stress. It is known that higher levels of stress in a lattice are conducive to twinning (33,34).

The effects of second phases remain largely unexplored. The presence of $FeBe_2$ in an Fe-25 atomic percent Be alloy does not inhibit twinning in the overaged condition, but when it exists as a finely dispersed "G.P. zones" twinning is totally supressed. Conflicting evidence leaves the effects of second phases on twinning unresolved (35,36).

The effects of particle coherency and crystallographic orientation is also unexamined. The availability of slip or twinning modes in shearable second phases ought to influence matrix deformation. The specific

effects ought to depend upon the crystallographic constraints imposed by precipitate morphology. In Ti-Mo and Ti-V where unusual twinning behavior is noted in the presence of the omega phase, certain factors related to the omega phase make comparison between the two alloys difficult. The omega phase in Ti-Mo is of the low misfit variety while in Ti-V it is of the higher misfit variety. One may intuit that certain deformation modes occur in Ti-Mo as a result of the easier ability to shear the omega phase, while the higher misfit in Ti-V may preclude the occurrence of the same modes in its alloys. Even though the crystallographic orientation is identical in these two alloys, factors such as the size and misfit may lead to differing deformation behavior.

In Ti-V alloys one may expect a limited number of possible interactions of a BCC twinning mode with the omega phase: (i) the particles may remain unsheared but bypassed, (ii) the particles may be sheared and reverted or reoriented, (iii) if the omega is reverted, an athermal retransformation of the atoms to the omega structure could occur after twinning. Each of these possibilities is accompanied by diffraction effects which can be observed in the electron microscope.

CHAPTER III

EXPERIMENTAL PROCEDURES

A series of titanium-vanadium alloys of nominal compositions 20, 24, 28, and 32% V by weight were prepared by arc melting starting materials of purity exceeding 99.92^{+}%. Tensile samples were machined from the homogenized cast and rolled blanks. After machining and thermal stress relief the samples were given thermal treatments selected on the basis of the precipitation parameters and hardness variations determined by previous investigators (4,21). The deformation substructure was examined utilizing optical and transmission electron microscopy to identify the observed deformation products.

Alloy Preparation

Each melt was prepared by arc melting the starting material in an MRC arc melter previously purged ten times with prepurified argon gas. To scavenge any residual oxygen, a Ti getter was melted in the purged atmosphere prior to the actual alloy preparation. Approximately 100 gram buttons were cast and remelted several times to insure adequate homogenization without disturbing the atmosphere of the melter. The buttons were finally cast into rods about 12x12x150 mm. Further homogenization and solutionizing treatments were accomplished by holding the vacuum encapsulated ingots for one week at 1000°C followed by quenching into icy brine. All thermal treatments were preceeded by vacuum encapsulating the degreased and chemically etched alloys in Vycor

or Pyrex tubing. The solutionized ingots were reduced about 50% in thickness by cold rolling and subsequently recrystallized at 875°C for one hour.

Tensile Specimen Preparation

Tensile samples were prepared similarly from the recrystallized blanks to conform to the ASTM subsize tensile geometry for 5 mm thick rectangular and 3 mm diameter cylindrical gage sections (41). Tensile tests were carried out on an Instron Testing machine with a strain rate of 10^{-2}/min.

Optical and Transmission Electron Microscopy

The deformed alloys were examined optically and by transmission electron microscopy (TEM). The rectangular samples were metallographically polished prior to deformation in order to observe the unetched deformation microstructures. Further optical microscopy was done by examination of transverse sections obtained near the fracture surface in the gage. After sectioning, the cut surface was polished and etched with an aqueous solution of 1.5% HF, and 3.5% HNO_3 by volume to reveal the deformation microstructure. Proper etching times depended on the sample solution composition, but generally required around thirty seconds etching to sufficiently resolve the deformation microstructure at room temperature. It was necessary to slightly overetch the surface to resolve the deformation products.

Parallel slices perpendicular to the gage tensile axis were obtained from the tensile samples, while slices of the rolled samples were obtained parallel to the rolling and normal directions. The 0.4-0.6 mm slices were

wet ground on 600 or 800 grit SiC paper to 0.17-0.25 mm thickness and 2.3 mm discs were mechanically punched out for TEM foils. The TEM samples were prepared by electrolytically dimpling the discs on both sides and finally electropolishing in another electrolyte until a penetration of a hole. It was found, particularly in the lower compositions, that optimum foils were obtained by allowing polishing to continue a few seconds after penetration of a hole. The dimpling electrolyte was 10% $HClO_4$(70%) and 90% methanol. The dimpling current was 150 ma at room temperature. The final polishing electrolyte was a perchloric acid, butanol and methanol solution used at -35 to -40°C with a polishing voltage of 13 volts (42).

The substructure of the foils was analysed by the standard TEM methods of bright field and dark field imaging, trace analysis and analysis of selected area diffraction (SAD) patterns. The use of these techniques as well as the general theory of image contrast and diffraction effects in metallic lattices is described by several authors (43-45).

CHAPTER IV

EXPERIMENTAL RESULTS

In order to assess the effect of variation of solute content on the microstructure and mechanical properties of these Ti-V alloys, samples were prepared from the solutionized alloy blanks and subsequently deformed either by cold rolling or tensile testing. Stress-strain curves were obtained from the raw load-elongation data. Determination of actual tensile behavior within the elastic and initial plastic regions was hampered by the "softness" of the Instron testing machine. The deformation microstructures were examined by optical and transmission electron microscopy (TEM).

The tensile samples were pulled to fracture in order to assess the overall ductility of the several thermal treatments. While tests to fracture indicate the certain alloy compositions and thermal treatments possess excellent ductility and allow adequate optical observation of the operative deformation modes; the analysis of the substructure by TEM is quite complicated. To aid in the TEM analysis of the substructure, the grip sections of the tensile specimen were examined in the electron microscope along with the gage sections. To further facilitate interpretation of the heavily deformed alloys' substructure, similar alloys reduced a few percent in thickness by cold rolling were examined by TEM methods. A comparison between the substructure of the grip sections of the tensile specimen and the rolled material established the reliability

of comparison of the microstructures produced by these two deformation processes. The two processes were found to produce similar microstructures arising from the same deformation mechanisms. The results are divided into the optical microscopy and tensile tests, and the TEM analysis of the resulting deformation substructure.

Tensile Tests and Optical Microscopy

The tensile curves and mechanical behavior of the experimental alloys in various microstructural states is presented in Tables 1 and 2, and Figure 3. The ductility varies from the embrittled behavior of the aged 20% vanadium alloy which failed at the initiation of yielding to the very ductile behavior of the Ti-24% V quenched and/or aged alloys. In Figure 3, the tensile behavior of the Ti-24% V alloy, in the quenched condition (curve 1), aged 1 hour @ 400°C (curve 2), 1 hour @ 300°C (curve 3), 11 hours @ 300°C (curve 4), and the Ti-32% V alloy in the as quenched condition (curve 5) and aged 0.5 hour @ 400°C (curve 6) illustrate the range of mechanical response to tensile loading within the experimental alloys. It can be seen that the as quenched and aged 1 hour at 300 and 400°C Ti-24% V alloys behave similarly, exhibiting increased strengths and decreasing elongations with increased omega volume fraction. The Ti-20 and 24% V alloys are observed to be remarkably ductile while the omega volume fraction is as high as 0.5. A coarse twin product is observed optically when an alloy contains omega, and predominant deformation by this coarse twin product is observed whenever the omega volume fraction is below about 0.6. It is noted that a "tin cry" indicative of twinning was heard in the Ti-24% V twinning alloys from the beginning of loading.

After plasiticity begins, marked load drops (indicated by vertical lines in Figure 3) and loud clicks were also heard. It is noted the mechanical behavior of the other alloys of higher solute content and lower maximum omega volume fraction varied little upon aging. The Ti-32% V alloy's tensile behavior illustrates this. The 32% V alloy ought to possess a volume fraction of omega no greater than about 0.3 while the as quenched condition is omega free. Neither alloy exhibits significant load drops or differing tensile behavior although a few coarse twins were observed optically in the aged alloy.

The deformation behavior of the quenched alloys is observed to be similar to that reported earlier (4). The tensile deformation behavior of the aged samples can be summarized utilizing the data of Hickman to determine the approximate omega volume fraction in each tested condition. With increased omega volume fraction no change in deformation mode is observed until it exceeds 0.6. In alloys containing less than 0.6 omega volume fraction, increased strength and slightly reduced ductility occur with increased omega volume fraction. The as quenched 24% alloy elongated about 50% to fracture while the alloy aged 1 hour at 300°C elongated about 37% to fracture. The ultimate tensile strength of these two conditions are about 6.8 and 8.0 x 10^8 n/m^2 respectively. The enhanced ductility of the as quenched alloy is manifested in a large reduction in gage area before fracture. It is also noted that the lower solute content alloys possessing significant omega volume fractions ($\lesssim 0.6$) possess better ductility and deform to a greater degree by twinning than the higher solute alloys which possess less omega volume fraction and deform primarily by slip.

Table 1. The Yield Stress (YS), Ultimate Tensile Strength (UTS), Strain at the Initiation of Necking, $\epsilon_N(\%)$, and Strain at Fracture, $\epsilon_F(\%)$, of Some Ti-V Alloys

Alloy and Thermal Treatment	YS ($\times 10^{-8}$ n/m^2)	UTS ($\times 10^{-8}$ n/m^2)	$\epsilon_N(\%)$	$\epsilon_F(\%)$
Ti-24% V				
As Quenched	4.5	6.5	32.5	48.3
1 hour @ 400°C	5.6	7.1	17.0	30.0
1 hour @ 300°C	5.9	7.95	35.0	35.0
11 hours @ 400°C	5.8	5.8	-*	1.0
Ti-32% V				
As Quenched	5.5	5.7	8.7	22.5
0.5 hours @ 400°C	5.5	5.7	8.7	18.0

*no necking prior to fracture

Table 2. A Summary of the Observed Microstructures and Deformation Characteristics of Beta Ti-V Alloys

Aging Temp.	Aging Time	Ti-20% V	Ti-24% V	Ti-28% V	Ti-32% V	Ti-36% V	Ti-40% V
400°C	As Quenched	B+O, Ductile CT*	B+O, Ductile CT*	B+O, Ductile CT*	B , Ductile Slip, FT	B , Ductile Slip, FT	B , Ductile Slip, FT
	0.17 hr.	B+O, Brittle Slip, CT	B+O, Ductile CT				
	0.33 hr.		B+O, Ductile CT				
	0.50 hr.				B+O, Ductile CT		
	0.75 hr.		B+O, Ductile CT				
	1.00 hr.		B+O, Ductile CT	B+O, Ductile CT			
	1.67 hr.	B+O+A, Slip FT	B+O+A, Slip FT,	B+O+A, Slip FT	B+O+A, Slip FT	B+O+A, Slip FT	B+O+A, Slip FT
300°C	1.00 hr.		B+O, Ductile CT				
	11.00 hr.		B+O, Brittle Slip, CT				

CT: Coarse Twinning, FT: Fine Twinning, B: Beta, O: Omega, A: Alpha
*Omega noted in as quenched samples

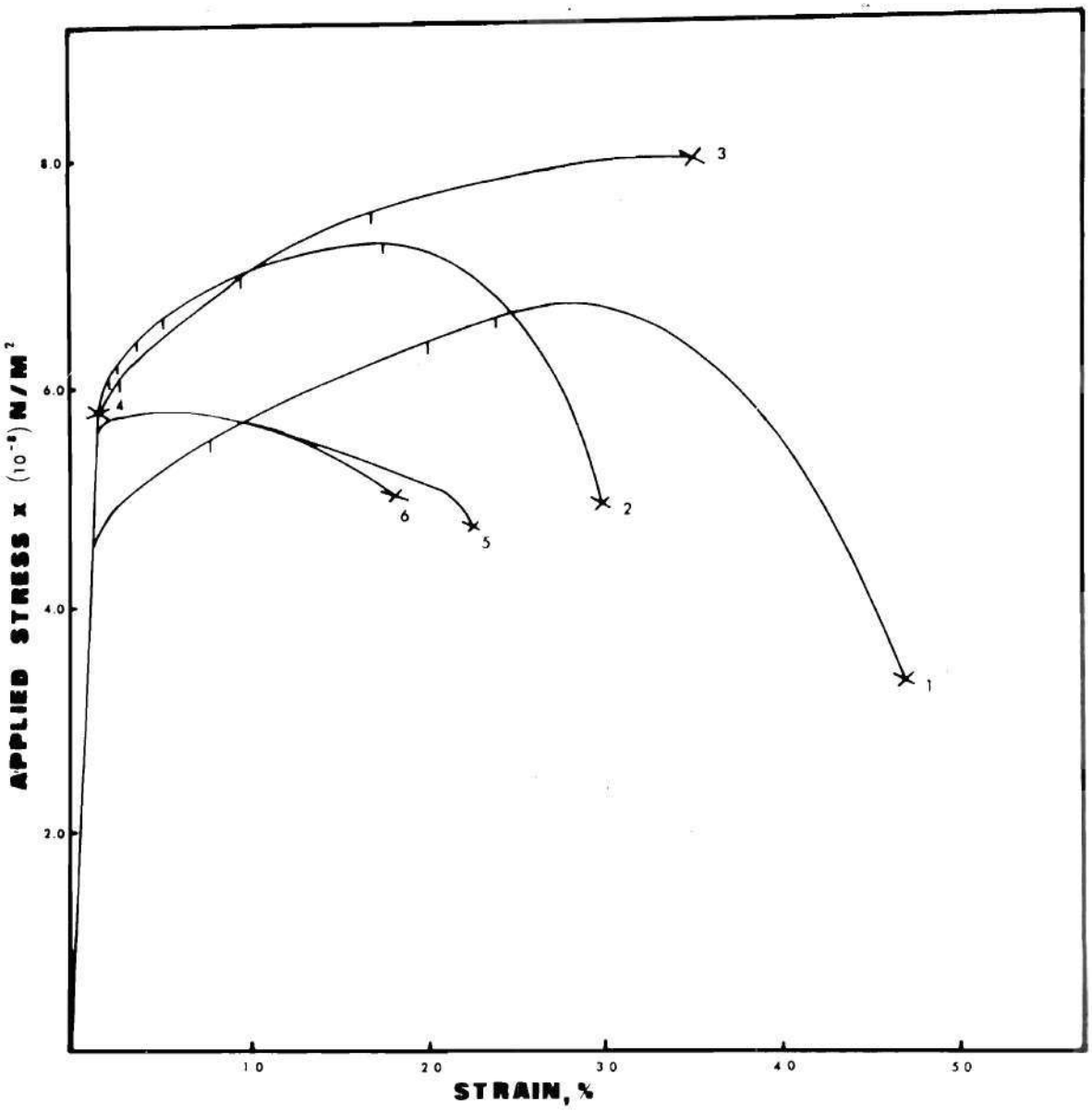

Figure 3. The Applied Stress vs. Strain Behavior of Some Ti-V Alloys

Figure 4 illustrates representative microstructures of the deformed as quenched Ti-20% V alloy. The surface of the prepolished gage (Figure 4a) reveals no indication of slip but does reveal large stress induced plates, marked "A" which have been identified as $\{\overline{1}12\}$ <111> deformation twins by TEM.

In Figure 4b, a metallographic section transverse to the gage tensile axis, details of the twinning can be seen. There is no evidence of slip, usually indicated by etch pitting along prominent slip lines. Close examination of Figure 4 reveals two characteristics of the deformation morphology. The plates appear to be composed of layers, as if the microscopic twin arises from repeated abutment of finer micro-twins (see the area marked "A" in Figure 4b for example). The other prominent feature of the microstructure is the great amount of internal twinning within the coarse plates (see the area marked "B" for example).

Samples of the same composition aged six or ten minutes at 400°C reveal a markedly different deformation behavior. The tensile tests show a marked reduction in ductility. In fact, the aged samples invariably failed upon, or shortly after the initiation of loading. Figure 5 is a series of micrographs of prepolished gage sections and metallographically prepared transverse gage sections. In the region of the fraction within the grip one can see that extensive planar slip has occurred leading to premature failure by crack initiation within the slip bands. Figure 5 illustrates the salient point that no observable evidence of twinning or slip exists outside the volume adjacent to the fracture surface. Although this sample failed by slip, coarse twinning has occurred around grip indentations (Figure 5c).

Tensile tests of the Ti-24% V alloy aged for various times up to 1 hour at 400°C and 11 hours at 300°C are singularly characterized by a pronounced and continuous "tin cry" and a discontinuous, but more pronounced, clicking at higher strains. The continuous clicking began virtually at the initiation of loading and persisted throughout the tests. This noise is to be differentiated from the loud, infrequent

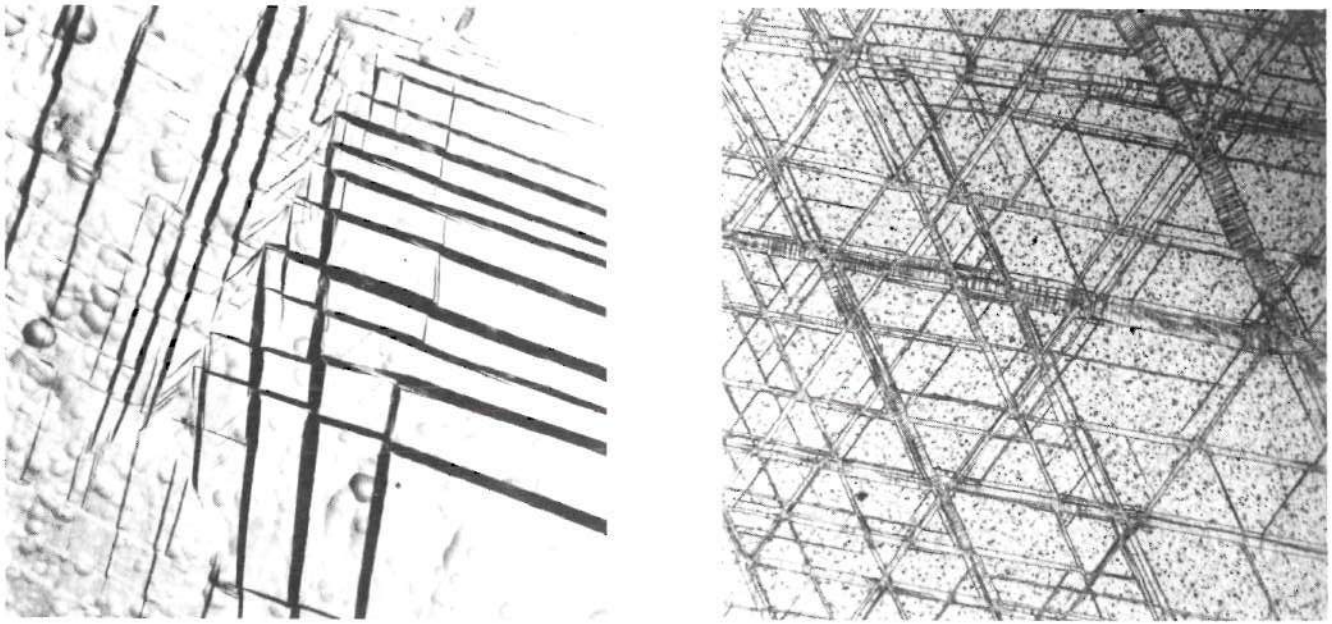

(a) (b)

Figure 4. The Tensile Deformation Microstructures in as Quenched Ti-20% V (150X) a) Prepolished Surface of the Gage, b) Polished and Etched Transverse Gage Section

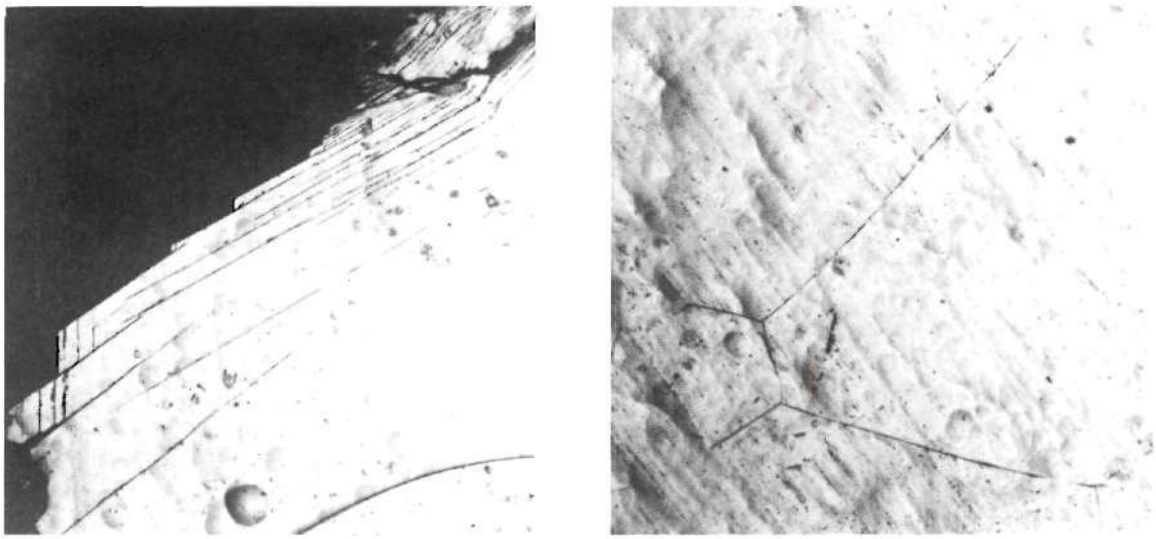

(a) (b)

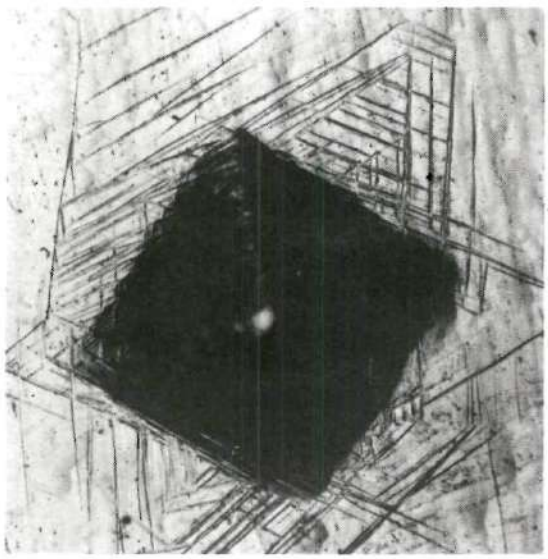

(c)

Figure 5. The Tensile Deformation Microstructures in Ti-20% V Aged 0.1 hr. @ 400% (150X) a) Prepolished Surface at Fracture in Grip Region, b) Prepolished Surface in Gage, c) Twinning at Grip Indentation

clicks associated with pronounced load drops in the load elongation record. The significance of this "tin cry" accompanying the discontinuous clicking occurring only in the Ti-24% V alloy is not fully understood; however, the continuous clicking is apparently related to the very fine size of individual twinning events. By noting the chart elongation reading at the onset of the "tin cry" the necessary strain for twinning in polycrystalline samples is estimated to be no greater than 0.1%. The optical microscopy of the Ti-24% V alloys reveal little difference in deformation microstructure between the various thermal treatments. Figure 6 presents deformation microstructures of the alloys with these treatments. As in the case of the as quenched Ti-20% V alloy, deformation occurs predominantly by twinning with little or no indication of slip.

It was desirous to observe lightly deformed microstructures and to compare the effects of similar volume fractions of omega in the Ti-24% V alloy with that produced in the Ti-20% V alloy aged 6 or 10 minutes at 400°C. Consequently, samples of the Ti-24% V alloy were aged at the lower temperature of 300°C for one and eleven hours and then rolled a few percent reduction in thickness ($\lesssim$ 8%). The one hour aging treatment produces a volume fraction and particle size comparable to a ductile thermal treatment in this alloy, 0.33 hr. @ 400°C. Figure 7 and 8 are representative polished and etched sections perpendicular to the rolling and normal directions of the one and eleven hours treatments, respectively. The deformation microstructure of the eleven hour treatment is comparable to the embrittled Ti-20% alloy microstructure. The deformation microstructure of the alloy with the one hour treatment is very similar to that observed in the previously mentioned alloy aged at 400°C. Although the

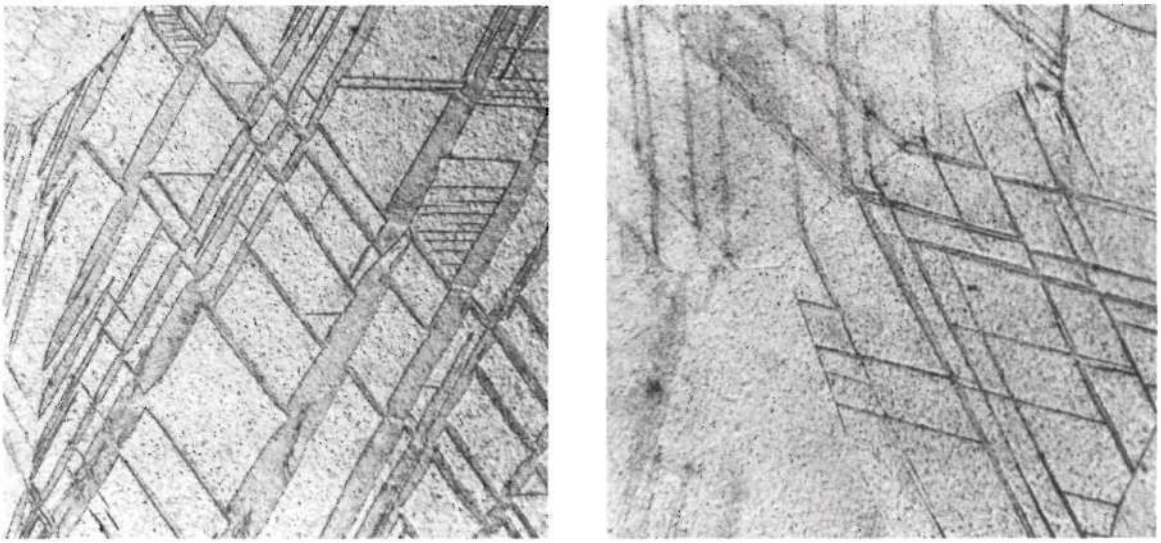

(a) (b)

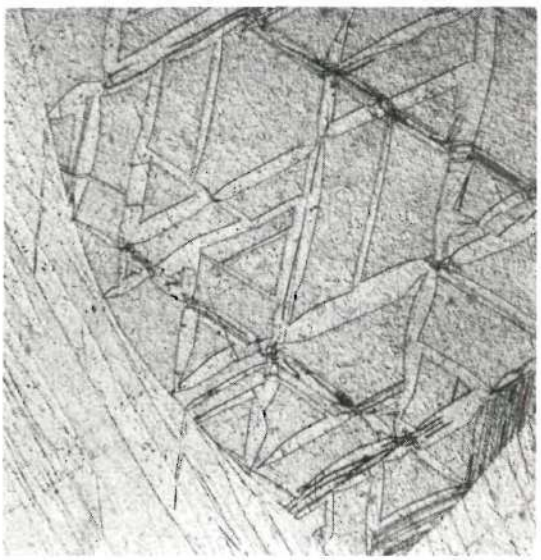

(c)

Figure 6. The Tensile Deformation Microstructure in as Quenched or Aged Ti-24% V Polished and Etched Transverse Gage Sections of: a) The as Quenched Alloy, b) The Alloy Aged 0.13 hr. @ 400°C, c) The Alloy Aged 0.33 hr. @ 400°C. (150X)

predominant deformation in the embrittled Ti-24% V alloy (Figure 7) is planar slip, close examination indicates coarse twinning has occurred. Figure 7b shows that twinning has occurred primarily in grains which appear less favorably oriented for slip and between slip bands. This micrograph also shows the probable mode of failure is cracking initiated within the slip bands.

The Ti-28% V alloy tested in the as quenched and aged one hour at 400°C showed little difference in deformation character. Both alloys produced virtually the same load elongation behavior. Although no continuous clicking or "tin cry" was heard, deformation in both conditions was accompanied by prominent clicks and load drops in the load elongation record. Figure 9 presents representative optical microstructures of transverse gage sections of deformed alloys of these two conditions.

The 32% V alloy tested in the as quenched and aged 0.5 hr @ 400°C displayed no difference in tensile behavior although the optical microstructure appears different. Figure 10 is a transverse gage section of the as quenched and the aged deformed alloys. There is no evidence of coarse twinning in the as quenched sample (Figure 10a). Only short rows of etch pits ("A" in Figure 10a) and fine twins ("B" in Figure 10a) are seen. The aged sample (Figure 10b) which possesses a low omega volume fraction has twinned to a greater extent. Some coarse twins are noted at "A" in Figure 10b. These two micrographs suggest coarse twinning does not occur in these alloys in the absence of the omega phase.

The optical microscopy of the tensile and rolled samples, and the observed tensile behavior reveal two basic characteristics of deformation in these alloys. The Ti-24% V alloys aged at 400°C and at one

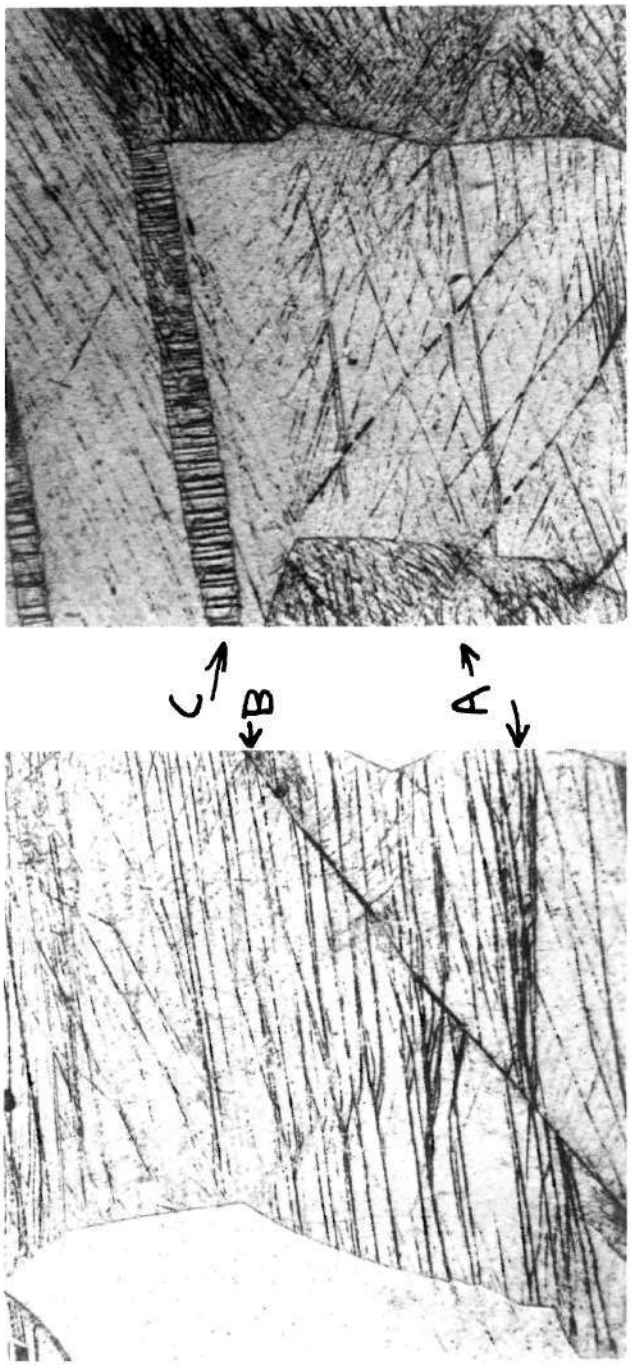

(a) (b)

Figure 7. Polished and Etched Sections of a Rolled Sample of Ti-24% V Aged 11 hrs. @ 300°C (150X) a) Illustrating Slip (A) and Cracking (B), b) Illustrating Slip (A) and Coarse Twinning (C)

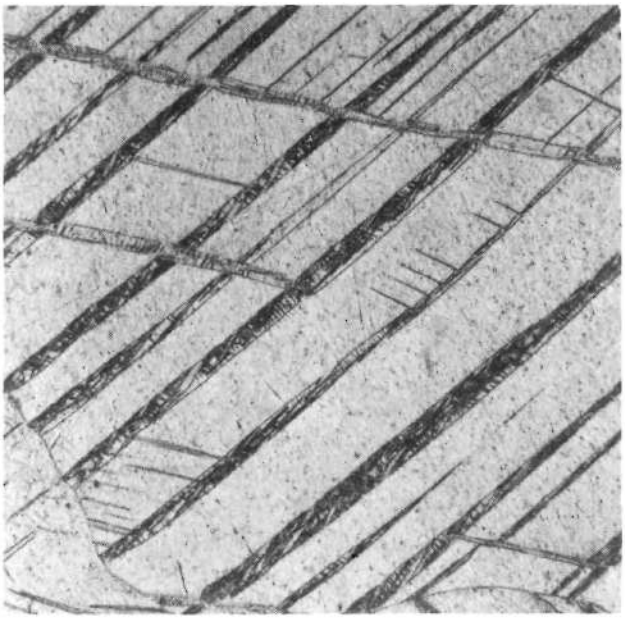

Figure 8. Polished And Etched Section of a Rolled Sample of Ti-24% V Aged 1 hr. @ 300°C, Showing Deformation Twinning (150X)

hour at 300°C and all aged experimental alloys of higher solute content, as well as the as quenched Ti-20% V alloy, exhibit marked ductility and deform predominantly by coarse $\{\bar{1}12\}$ <111> twinning with little accompanying slip. The aged Ti-20% V alloy and the Ti-24% V alloy aged eleven hours at 300°C are embrittled and deform predominantly by planar slip. Small amounts of coarse twinning are observed in the embrittled alloys.

TEM Analysis

TEM analysis of the deformation substructure was undertaken to establish conclusively the crystallographic identity of the deformation product and the interaction of the twinning with the omega phase. This interaction varied with solute content and aging condition. Due to the large amounts of internal deformation of the twins as a result of "emissary"

(b)

(a)

Figure 9. The Tensile Deformation Microstructures in Polished as Quenched or Aged Ti-28% V (150X) a) As Quenched, b) Aged 1 hr. @ 400°C

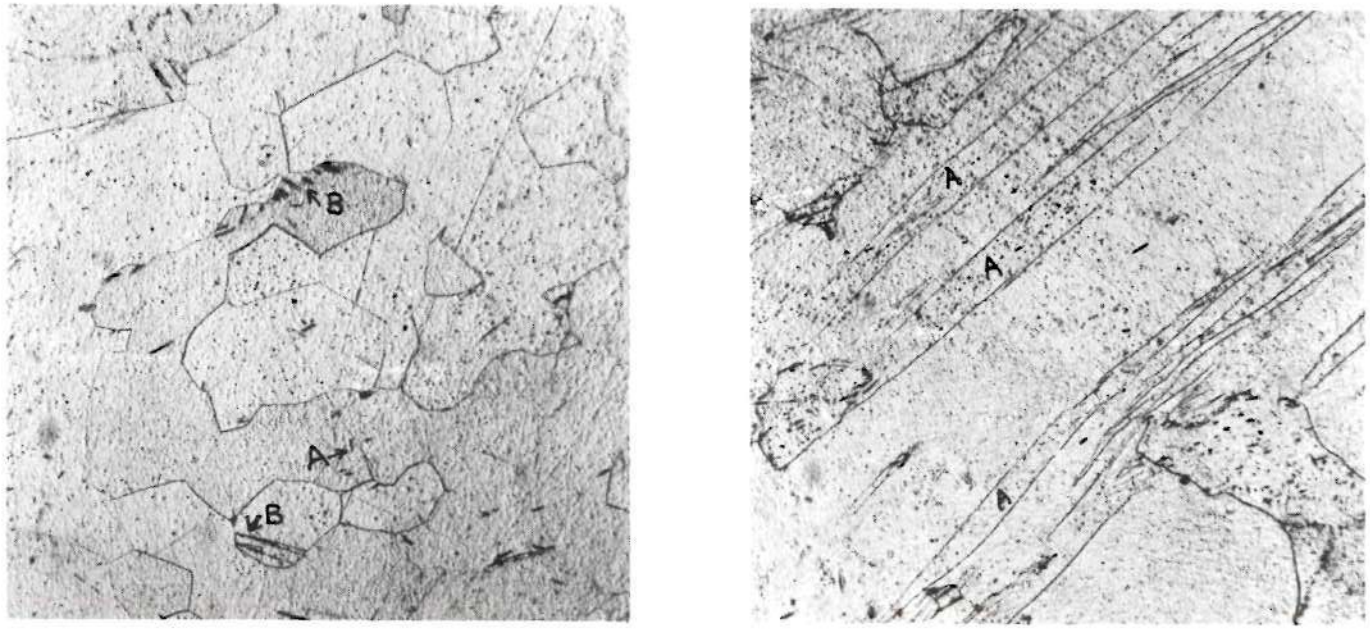

(a) (b)

Figure 10. Tensile Deformation Microstructures in As Quenched or Aged Ti-32% V (150X)
a) As Quenched, b) Aged 0.5 hr. @ 400°C

slip and internal twinning, as well as foil relaxation effects, conclusive identification of coarse twin boundaries was not always achievable. It is noted that the large width of the twins often made it impossible to *determine whether the analysis was being done within the matrix or* coarse twin. This in itself lends support to some of the arguments used in the next chapter to explain the observed twinning. In other words, the inability to differentiate matrix and twin suggests a similar alloy structure exists in both.

Analysis of SAD patterns from the twin/matrix boundaries in Figure 11 establish the identity of the coarse twinning as $\{\overline{1}12\}$ <111> twins. Matrix omega and beta reflections are noted with "O" and "B" subscripts respectively, while beta twin reflections are noted "T". The numbers in the subscripts of omega reflections indicate the specific orientation variant as identified in Appendix II. These patterns also illustrate some of the complications of analysis of microstructures containing both omega and $\{\overline{1}12\}$ <111> twins. SAD patterns taken of twin/matrix interfaces contain twin reflections whose positions mimic the spot positions of certain omega orientation variants' reflections. As a result, a pattern may be incorrectly indexed if it contains omega reflections of lesser intensity than the twin reflections. This situation often arises in practice because the twin diffraction volume is usually more favorably oriented for good diffraction. One can easily overlook the omega reflections not coincident with twin reflections in Figure 11.

Utilizing the crystallographic relationships of Appendix II, the spot positions of the four omega orientation variants in BCC SAD patterns can be established. In Figure 11a the cubic zone axis is 120. $\{\overline{1}12\}$ <111>

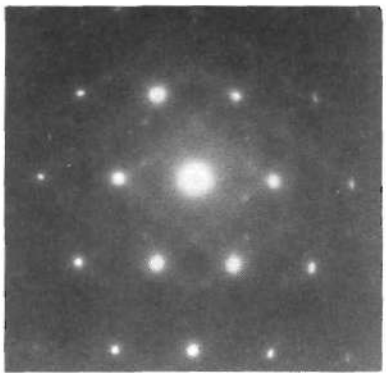

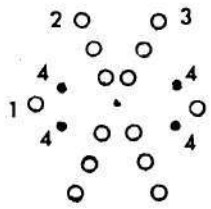

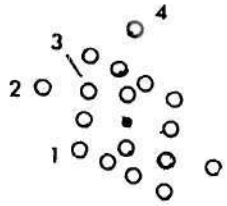

(a)

(b)

1: $(00\bar{2})_B$; $(0\bar{2}21)_{0,1}$; $(20\bar{2}1)_{0,2}$; $(\bar{2}021)_{0,3}$; $(02\bar{2}1)_{0,4}$

2: $(\bar{2}1\bar{1})_B$; $(3\bar{1}2\bar{1})$; $(\bar{2}13\bar{1})_{0,2}$; $(0\bar{1}1\bar{2})_{0,3}$; $(3\bar{3}00)_{0,4}$

3: $(\bar{2}11)_B$; $(3\bar{3}00)_{0,1}$; $(0\bar{1}1\bar{2})_{0,2}$; $(\bar{2}13\bar{1})_{0,3}$; $(3\bar{1}2\bar{1})_{0,4}$

4: $\{10\bar{1}1\}$ Omega from 110 Beta Zone

1: $(110)_B$; $(2\bar{1}\bar{1}0)_{0,1}$; $(\bar{1}011)_{0,2}$ $(\bar{1}01\bar{1})_{0,3}$; $(2\bar{1}\bar{1}0)_{0,4}$

2: $(\bar{1}12)_B$; $(2\bar{3}1\bar{1})_{0,1}$; $(10\bar{1}2)_{0,2}$ $(\bar{3}030)_{0,3}$; $(21\bar{3}\bar{1})_{0,4}$

3: $(110)_{BT}$; $(10\bar{1}1)_{0,2}$

4: $(1\bar{1}2)_B$; $(\bar{2}13\bar{1})_{0,1}$; $(30\bar{3}0)_{0,2}$ $(\bar{1}012)_{0,3}$; $(\bar{2}3\bar{1}\bar{1})_{0,4}$

Figure 11. SAD Pattern Analysis Showing the Identity of the Coarse Twins as $\{\bar{1}\bar{1}2\}$ <111> a) A 120 SAD Pattern Taken Within a Coarse Twin in Ti-24% V Aged 0.1 hr. @ 400°C Prior to Deformation b) A 110 SAD Pattern of Matrix and $\{\bar{1}\bar{1}2\}$ <111> Twins in Deformed Ti-28% V Aged 1 hr. @ 400°C Prior to Deformation

twin reflections arise from twinning on the (211), $(\bar{1}\bar{2}1)$, or $(1\bar{1}2)$ $[\bar{1}11]$ in all positions equivalent to 1/3 $[\bar{1}\bar{2}1]$ translations from cubic matrix reflections. When double diffraction from twin boundaries is considered, these reflections exist in all positions equivalent to 2/3 $[\bar{1}\bar{2}1]$ translations from cubic matrix reflections. Thus certain cubic {112} reflections are divided into thirds by the noncoincident twin primary and double diffraction reflections. As well, all omega reflections not coincident with matrix reflections divide the cubic {112} reflections into thirds. This results because the $(3\bar{3}00)$ reflection from omega orientation variant 2 coincides with the $(\bar{1}\bar{2}1)$ reflection. Other omega orientations possess similar relations with the remaining {112} reflections. The $(2\bar{2}00)$ and $(1\bar{1}00)$ always third the {112} reflections. Since {112} twinning planes possess similar relationships to other omega orientation variants, any omega reflection noncoincident with the matrix cubic reflections may be confused or obscured by the superposition of occurring $\{\bar{1}\bar{1}2\}$ <111> twin reflections. Although this illustration utilized {112} reflections, similar results apply for other cubic reflections when both twin and omega allow noncoincident reflections with the matrix reflections. The particular superposed spots obviously depends on the observed zone axis and specific {112} twin mirror plane.

Dark field images made with potentially superposed twin and omega reflections are a critical method to determine the nature of the microstructure contributing to the observed diffraction phenomena. This is often the only way to verify that omega reflections exist along with cubic $\{\bar{1}\bar{1}2\}$ <111> twin reflections. If the spot is composed of diffracted intensity from both omega and twin, the dark field image will illuminate

both. Without this technique, the only other way to verify spot superposition is by careful measurement of the relative intensity of diffraction spots. Anomolous differences in intensity from features more favorably oriented for diffraction than others can confound such measurements.

Figure 12 clearly illustrates the usefulness of dark field (DF) imaging to resolve the question of the existence of omega within the coarse twins. This micrograph is a DF image of a coarse $\{\overline{1}12\}$ <111> twin matrix in a Ti-24% V alloy aged 1 hour @ 300°C prior to rolling. The twinned region is the illuminated region comprising most of the micrograph. The accompanying 113 zone axis was taken entirely within the twin. Secondary twinning (the spotty, linear features running from left to right) and omega contribute to the extra diffraction spots in the pattern. As indicated in the SAD pattern analysis in Figure 13, the DF image is made with the superposed $(1\bar{1}01)$ reflection (from omega orientation variant 3) and a (011) cubic twin reflection. The image (11a) clearly shows both particles in the twin matrix and the secondary twinning are contributing to the observed diffraction. The primary twin is heavily dislocated making the omega particle morphology difficult to resolve. Nevertheless, distinct omega particles can be seen. The uppermost secondary twin (closest to the matrix/twin boundary) shows a distinct interaction between the twinning dislocation at its head and the omega particles in the primary twin matrix. Note that all omega orientation variants can be accounted for in the SAD pattern in Figure 13. This micrograph and SAD pattern establish the existence of multiple omega orientation variants within the coarse twins in ductile Ti-24% V alloys.

Although Figure 12 establishes the presence of multiple orientations

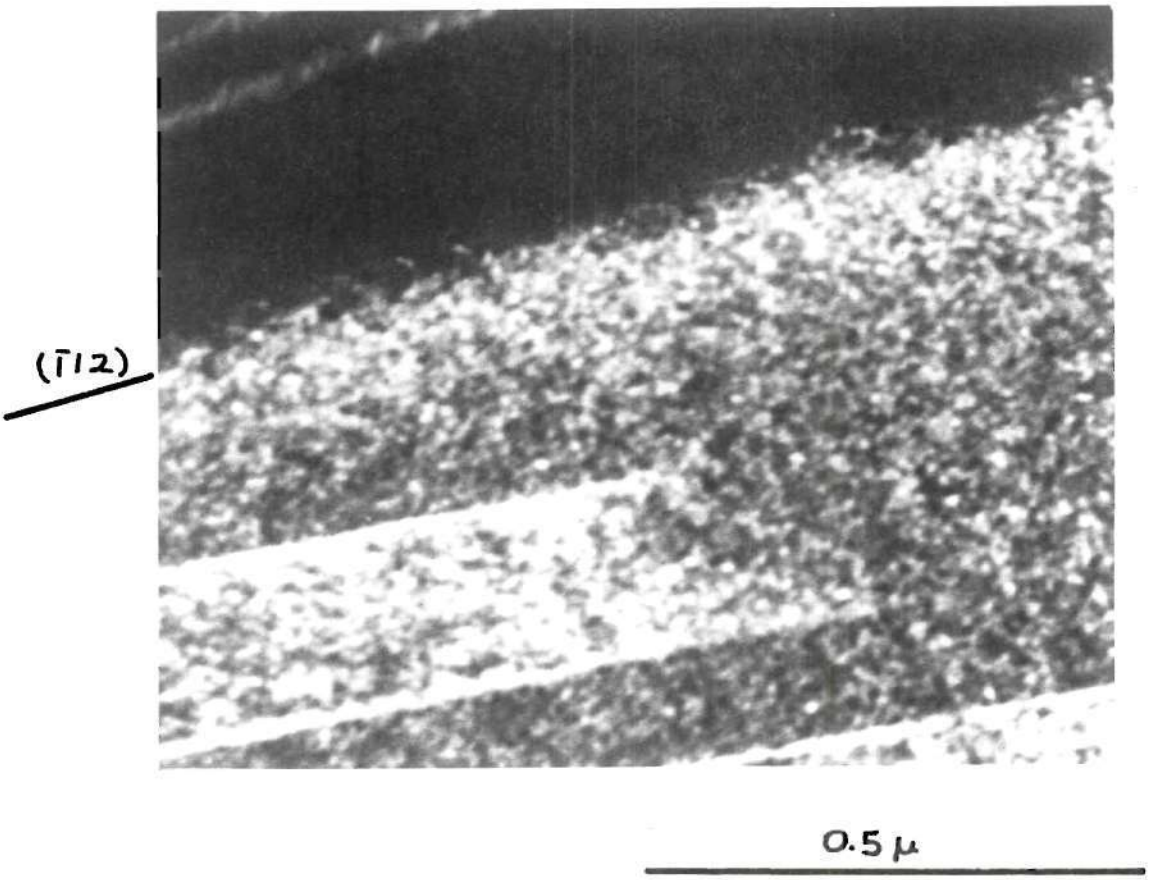

(a)

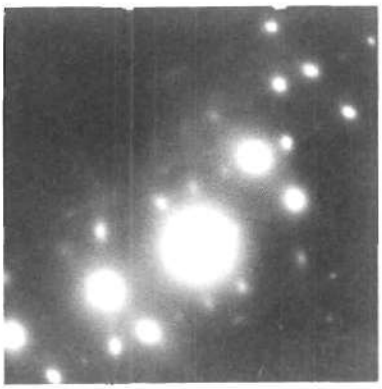

(b)

Figure 12. An Illustration of the Presence of Multiple Orientation Variants of the Omega Phase Within $\{\bar{1}\bar{1}2\}$ <111> Coarse Twins in Ti-24% V Aged 1 hr. @ 300°C Prior to Deformation. a) A Dark Field Image Using $\bar{g} = (11\bar{2}1)_{w3}$ b) The SAD Pattern Showing the 113 Zone Axis Obtained From The Twin in (a)

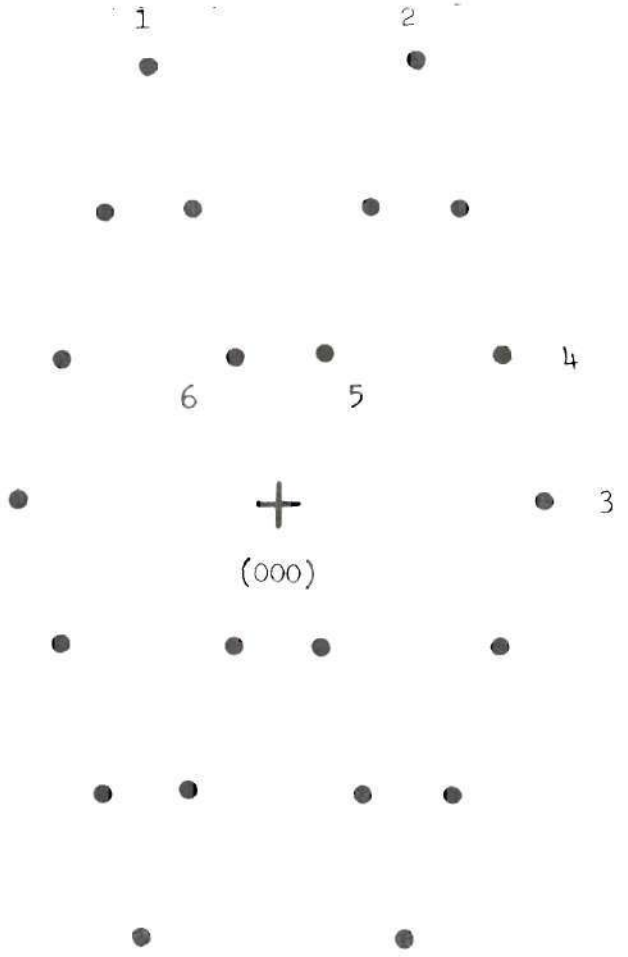

1:	$(\bar{2}11)_B$	2:	$(\bar{1}21)_B$	3:	$(1\bar{1}0)_B$	4:	$(01\bar{1})_{B,T}$
	$(1\bar{3}21)_{0,1}$		$(\bar{1}231)_{0,1}$		$(\bar{2}110)_{0,1}$		$(\bar{1}12\bar{1})_{0,3}$
	$(2\bar{3}11)_{0,2}$		$(3\bar{3}00)_{0,2}$		$(10\bar{1}\bar{1})_{0,2}$	5:	$(1\bar{1}00)_{0,2}$
	$(03\bar{3}0)_{0,3}$		$(1\bar{3}21)_{0,3}$		$(10\bar{1}1)_{0,3}$	6:	$(\bar{1}10)_{B,dd}$
	$(1\bar{1}02)_{0,4}$		$(\bar{1}01\bar{2})_{0,4}$		$(\bar{2}110)_{0,4}$		$(0\bar{1}10)_{0,3}$

Figure 13. The 113 Beta Zone Axis of the $\{\bar{1}\bar{1}2\}$ <111> Coarse Twin in Figure 11. The DF Image of Figure 11b is Made With Spot 4, the Superposed Reflection from Omega Orientation 3 and the Beta Secondary Twin.

of omega in the Ti-24% V alloy, it is not clear from the experimental results that similar conclusions are applicable to higher solute content alloys. The SAD evidence in the Ti-28% V alloys establishes the fact that omega is produced upon aging at 400°C, but that, at most, one orientation variant exists within the $\{\overline{1}12\}$ <111> coarse twins. Figure 14-16 are representative micrographs and SAD patterns of the aged and deformed Ti-28% V alloy.

Figure 14b and 15d are SAD patterns from twinned areas in these two micrographs. Although no coarse twin boundary exists, the fine scale microtwinning which eventually results in the coarse twin development do exist. The nature of the omega within these microtwins is expected to be the same as within these microtwins is expected to be the same as within the coarse twins. These 221 matrix zone axes contain a 100 twin zone in which omega and twin reflections are noncoincident with the matrix reflections. The twin and omega reflections are superposed. Examination of Figures 15 and 16, DF images made with superposed omega and twin reflections as indicated, show that the microtwin bands and single omega orientation variants are contributing to the superposed diffraction. The omega orientation variant whose reflections are superposed with the twin reflections appears to be that orientation whose $\bar{c}$ axis is parallel to the <111> twin shear direction. Figure 16 is a DF image of a region directly adjacent to the left hand part of Figure 15. This image is made with a superposed matrix, twin and omega reflection; however all the omega orientation variants contribute to this spot intensity and consequently are illuminated in DF. This micrograph shows that other omega orientation variants exist in regions not twinned, and that other $\{112\}$ <111> twins

also have single orientation variants associated with them. The evidence in these micrographs of the Ti-28% V alloy strongly suggest than no more than one omega orientation variant exists within the microtwins. Since the twin/omega reflections are coincident, if the prior omega particles were transformed to the twinned BCC structure, the microstructural appearance in DF would be similar until after the twinned volume increased in size. In other words, one could be viewing small twins which were previously omega particles. One also notes an obvious interaction of dislocations with the omega particles (see Figure 15 and 16).

The large twins observed optically do not appear to have arisen by single twinning events, but rather appear to have arisen by the abutment of many microtwins such as those seen in Figure 14-16. The load elongation record, especially that of the Ti-24% V alloy which exhibited the fine scale "tin cry", suggests the twins arise in this manner. TEM analysis of the substructure reveals evidence supportive of this conclusion. Figure 17 is a TEM micrograph of a Ti-24% V alloy aged 0.33 hr. @ 400°C prior to deformation. It is to be compared with the optical micrograph, Figures 4b and 6c. One should particularly note the sites "A" and "B" in Figure 6c. Figure 18 a micrograph of a TEM foil from a Ti-28% V alloy aged 1 hr. @ 400°C and deformed in tension shows a $\{\overline{112}\}$ <111> deformation twin which clearly is composed of many layers of fine microtwins of the same mode. No details of dislocation contrast can be seen because the operating reflections leave the dislocations out of contrast, but at "A" one can see the head of individual bands which are enlarging the width of the twin. The twins seen in Figure 6c, 17, and 18 leave little doubt that the method of coarse twin build up is repeated layering or abutment of

(a)

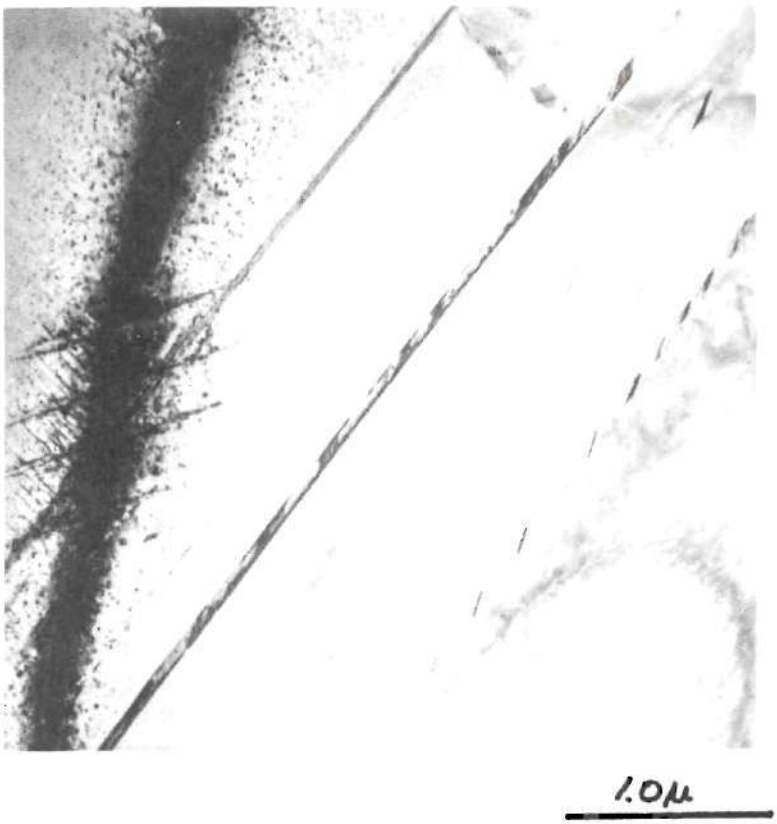

(b)

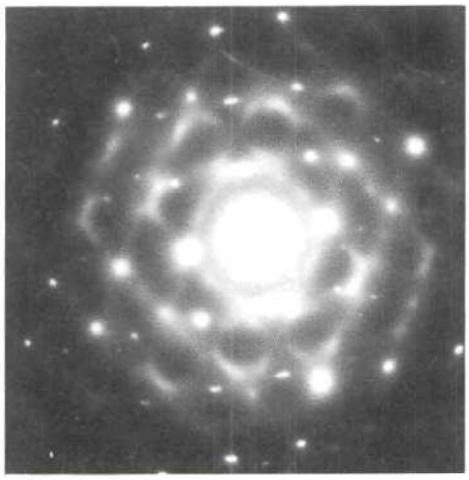

Figure 14. a) Propagation of $\{\bar{1}12\}$ <111> Microtwins From the Rod Structure by Dislocation Slip in Ti-28% V Aged 1 hr. @ 400°C. The Microtwin Bands are Parallel to $(\bar{1}21)$ and the Rods are Parallel to either [111] or $[11\bar{1}]$ b) 221 SAD Pattern

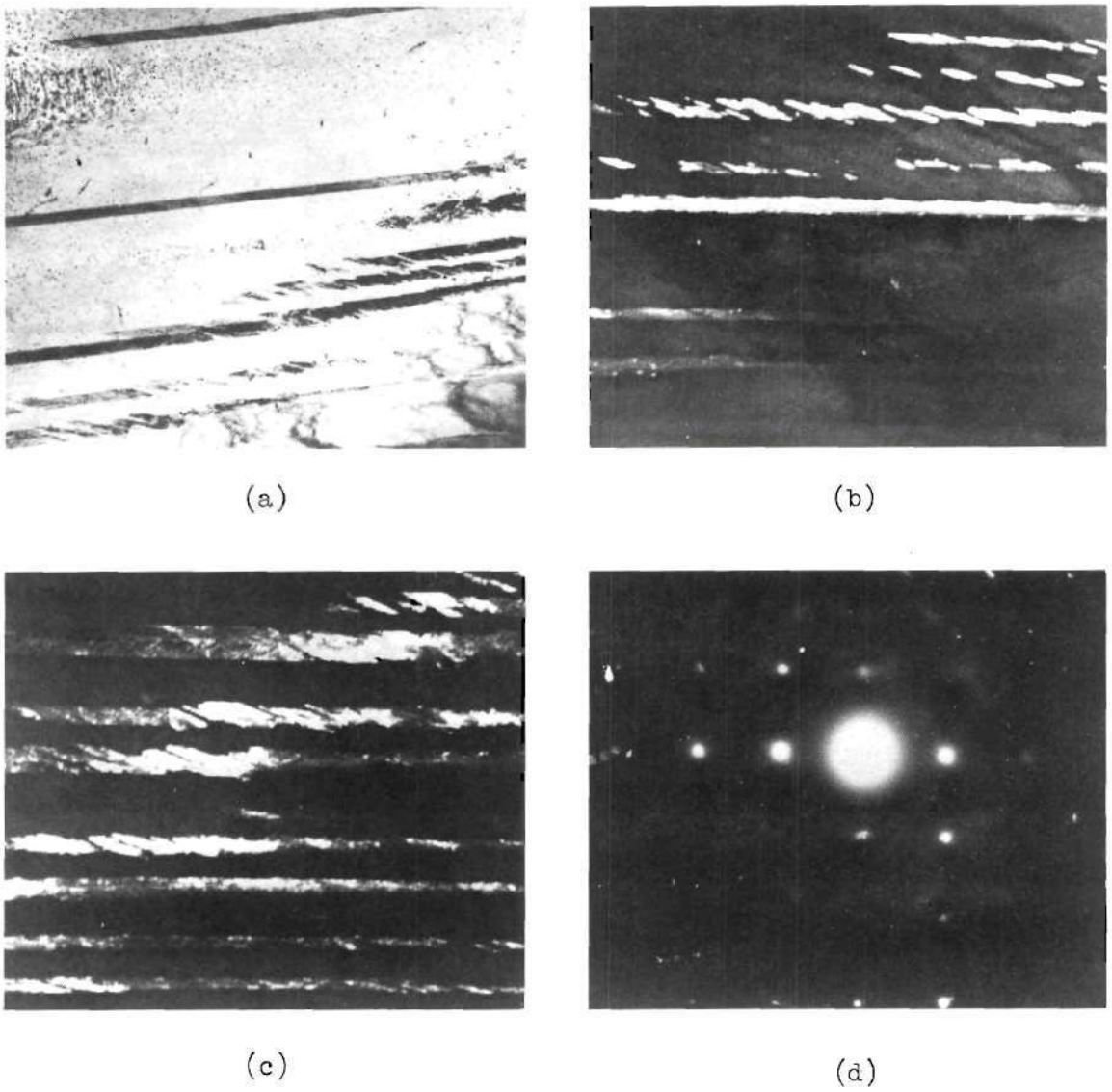

Figure 15. $\{\bar{1}\bar{1}2\}$ <111> Microtwins in Ti-28% V Aged 1 hr. @ 400°C. a) Bright Field, b) Dark Field, $\bar{g} = (01\bar{1}1)_{W4}$; $(110)_{bt}$, c) Dark Field, $\bar{g} = (20\bar{2}1)_{24}$; $(200)_{bt}$, d) SAD pattern, [221] Zone Axis

Figure 16. A Dark Field Micrograph of an Adjacent Area to Figure 14, Illustrating the Presence of Multiple Orientation Variants of Omega, $\bar{g} = (1\bar{1}0)_\beta$

microtwins of the same mode.

Figures 14-16 also reveal the interesting relationship between the omega orientation variants and the $\{\bar{1}\bar{1}2\}$ <111> microtwins, as well as the relationship of the "rods" and the microtwins. Previous discussion has pointed out that the existing omega orientation variant within the microtwins and rods is the one whose $\bar{c}$ axis is parallel to the <111> twin shear direction. At the same time these micrographs show the rod like features have the same unique relationship to the twins as do the omega orientation variants. These rods appear to contain the omega particles

(a)

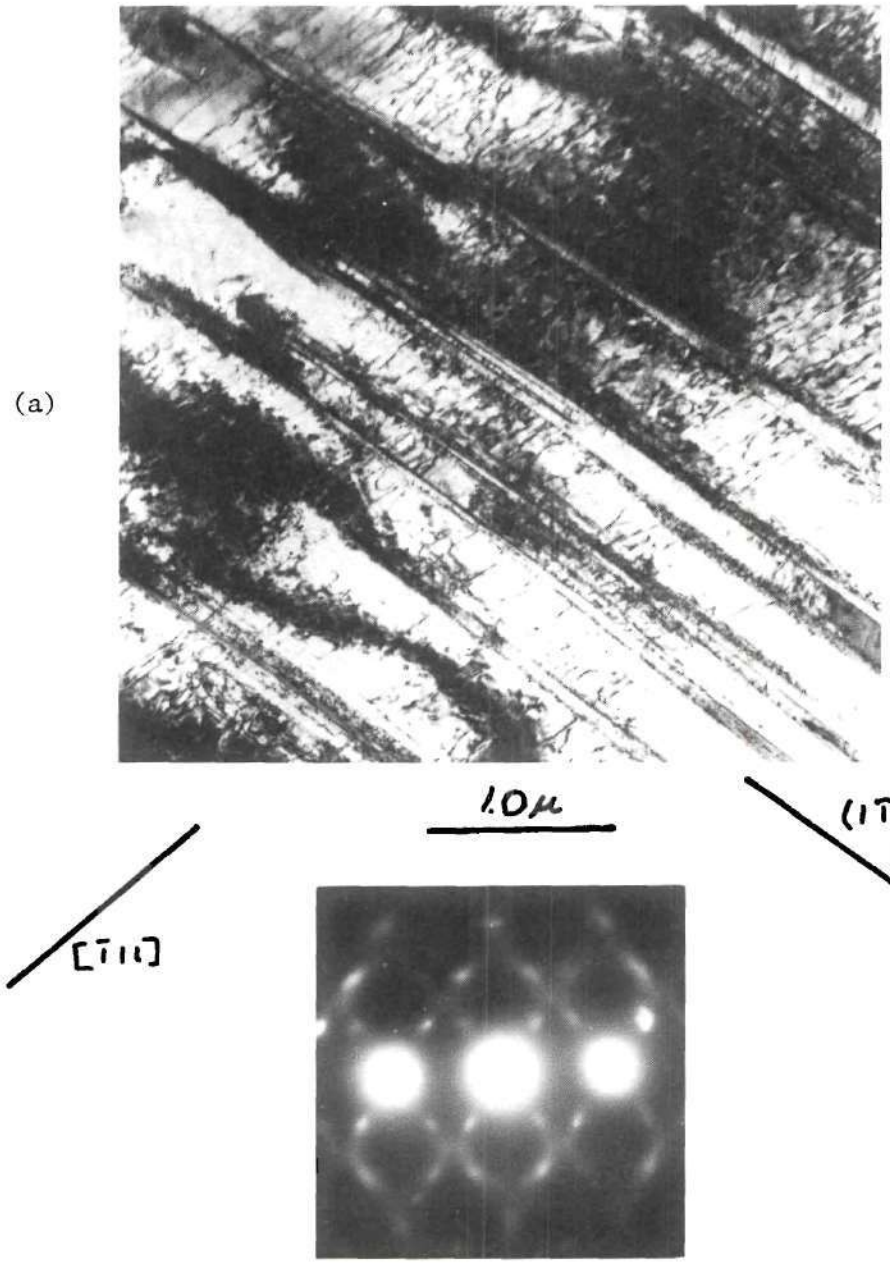

(b)

Figure 17. An Illustration of the Layering of $\{\overline{112}\}$ <111> Microtwins in Ti-24% V Aged 0.33 hr. @ 400°C Prior to Deformation, b) the SAD Pattern

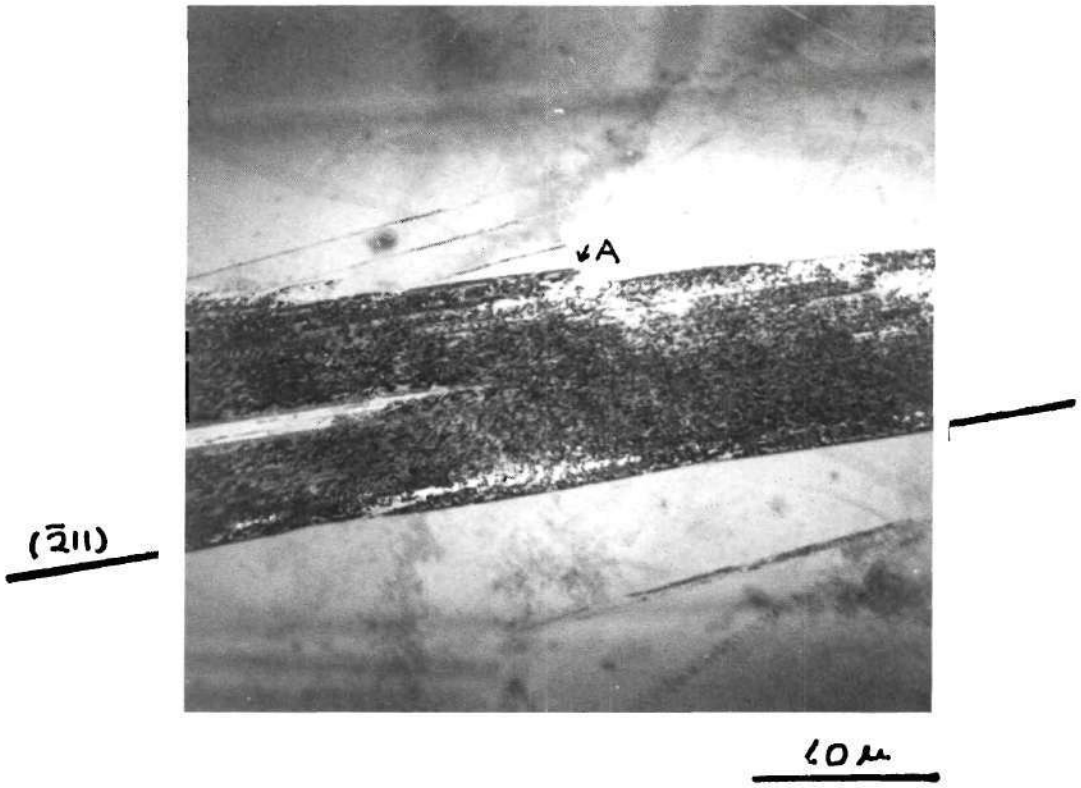

Figure 18. $\{\bar{1}12\}$ <111> Coarse Twin Build up by Repeated Layering of $\{\bar{1}12\}$ <111> Microtwins in Ti-28% V Aged 1 hr. @ 400°C

and to serve as the sites for nucleation and propagation of the $\{\bar{1}12\}$ <111> microtwin bands. Careful examination of the rods in Figures 14a and 15b,c show that dislocation motion from the rods is creating the twin bands. The preceding observations make unavoidable the conclusion that the coarse twins arise from repeated layering of the fine microtwin bands. The microtwin bands appear to arise as a result of twin nucleation at the rod like structure in association with the single omega orientation variant whose $\bar{c}$ axis is parallel to the twin shear direction.

The TEM analysis of the embrittled alloys reveals an entirely different substructure. The substructure observed by TEM is identical with that observed optically. Figure 19 is a representative micrograph

of the deformed, embirttled alloy, Ti-24% V aged 11 hours at 300° C. Slip and twinning are present within the microstructure; however, the predominant mode of deformation is clearly planar slip. The SAD pattern establishes the existence of multiple orientations of omega within the microstructure. It can be seen that deformation is confined to the slip bands. From these observations it is concluded that the predominant mode of deformation is slip and that the embrittled nature of the alloys arises from repeated slip within the limited volume of the slip band. Failure occurs as a result of the heterogeneous nature of the deformation, not because the alloy is microscopically embrittled. It is noted the coarse twinning has not disappeared as coarse twins are observed infrequently in the optical micrographs. Twinning has been limited to a minor process in the embrittled alloy.

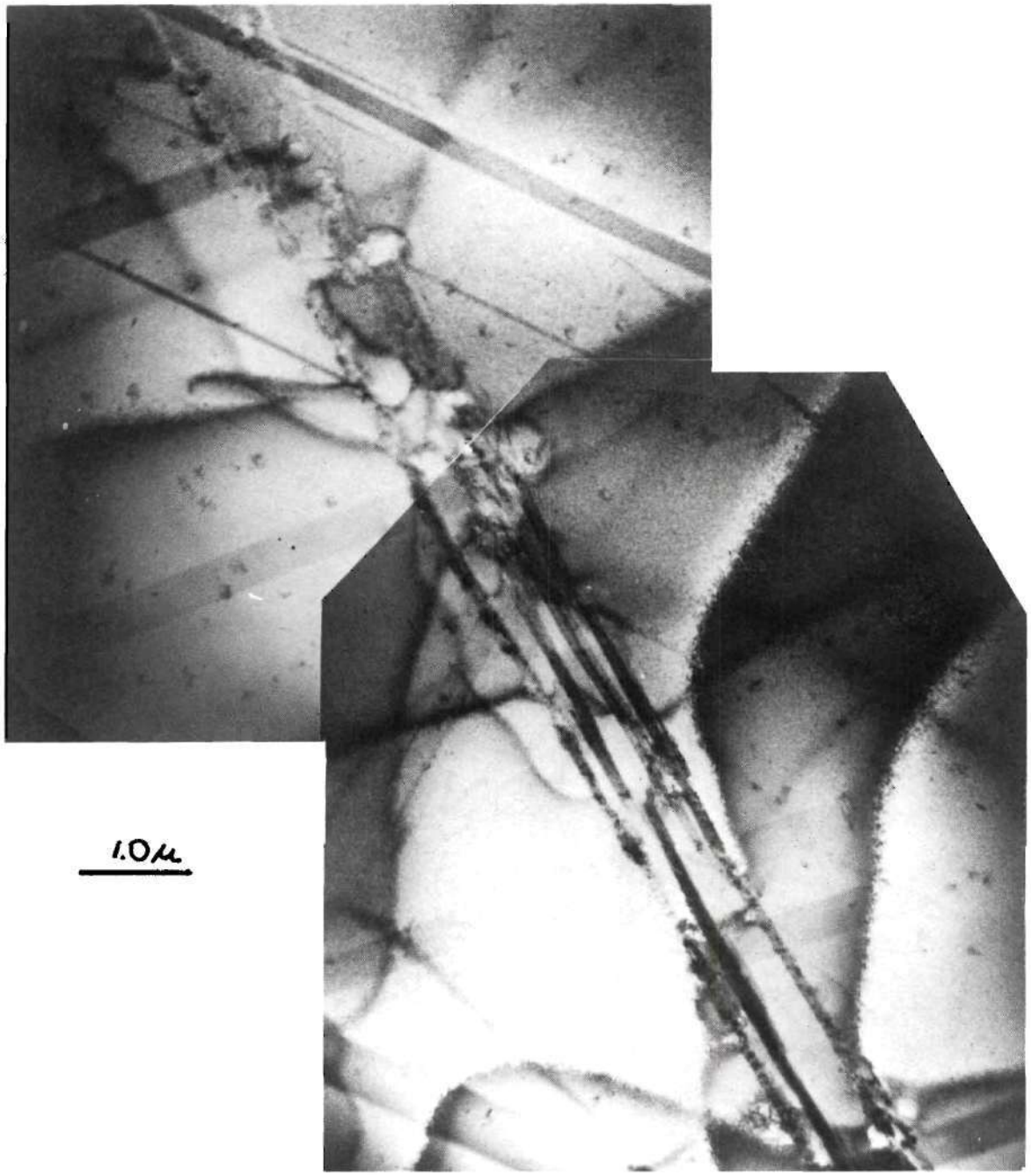

Figure 19. Slip Band Formation in a Cold Rolled Sample of Ti-24% V Alloy Aged 11 hrs. at 300°C, Bands are Parallel to (112) and ($\bar{1}$1$\bar{2}$).

CHAPTER V

DISCUSSION OF THE RESULTS

The experimental results of this study indicate that significant alteration of deformation behavior of Ti-V alloys can be obtained by variation of solute content and thermal treatments. It appears the presence of the omega phase is primarily responsible for this result, although the interaction of twinning and the omega phase appears to vary with solute content. Understanding the influence of the omega on deformation behavior necessitates a knowledge of the variation of omega precipitation parameters with aging time and temperature, as well as the omega crystallography. Table 3 presents the omega particle size, misfit and volume fraction for the Ti-20 and Ti-24% V alloys after aging at 300 and 400°C. Figure 20 presents the maximum omega volume fraction for specific aging times and temperatures. From inspection of these data, it can be seen that the mechanical response to applied stress in these alloys is closely correlated with the omega volume fraction. In the various thermal treatments over the experimental compositional range, the particle size and misfit vary slowly or remains constant while the omega volume fraction varies rapidly. It is reasonable to conclude that for constant particle size, the misfit produces only secondary effects if coherency is preserved, while the influence of volume fraction of omega is primary in effecting a change in deformation behavior from twinning and ductile yielding to slip and embrittled failure.

By comparing the data of Table 1-3 and Figure 20, one notes the presence of moderate amounts of omega product both marked ductility and coarse $\{\overline{1}12\}$ <111> twinning as the predominant deformation characteristics. There appears to be the necessity of the presence of the omega phase to induce the coarse twinning, although the absolute minimum value of volume fraction is not determined in this study. It is noted that the two tested Ti-32% V alloys exhibit a different appearing deformation microstructure depending on whether the sample has omega (aged sample) or not (quenched sample). Consideration of Hickman's data on variation in maximum volume fraction (Figure 20) at various solute contents suggests that after aging at 400°C the maximum volume fraction at 32% V is about 0.2-0.3. Predominant deformation by course twinning is observed for all thermal treatments producing omega volume fractions below the broken line in Figure 20. In alloys containing greater than about 0.6 omega volume fraction, a transition in major deformation mode to concentrated slip

Table 3. Some Precipitation Parameters of Ti-20 and Ti-24% V After Aging at 300°C or 400°C

Aging Treatment	Omega Volume Fraction	Particle Size	Misfit, $\bar{a}_0$	Misfit, $\bar{c}_0$	Vanadium Content Beta	Vanadium Content Omega
0.1 hr. @ 400°C, Ti-20% V	0.7	100Å			20%	20%
Ti-24% V, 1 hr. @ 400°C	0.5	100Å	-1.8%	-1.4%	30.5%	17.5%
1 hr. @ 300°C	0.4	85Å	-1.1%	-1.4%	24.6%	23.1%
11 hr. @ 300°C	0.7	97Å	-1.8%	-1.4%	33.3%	20.0%

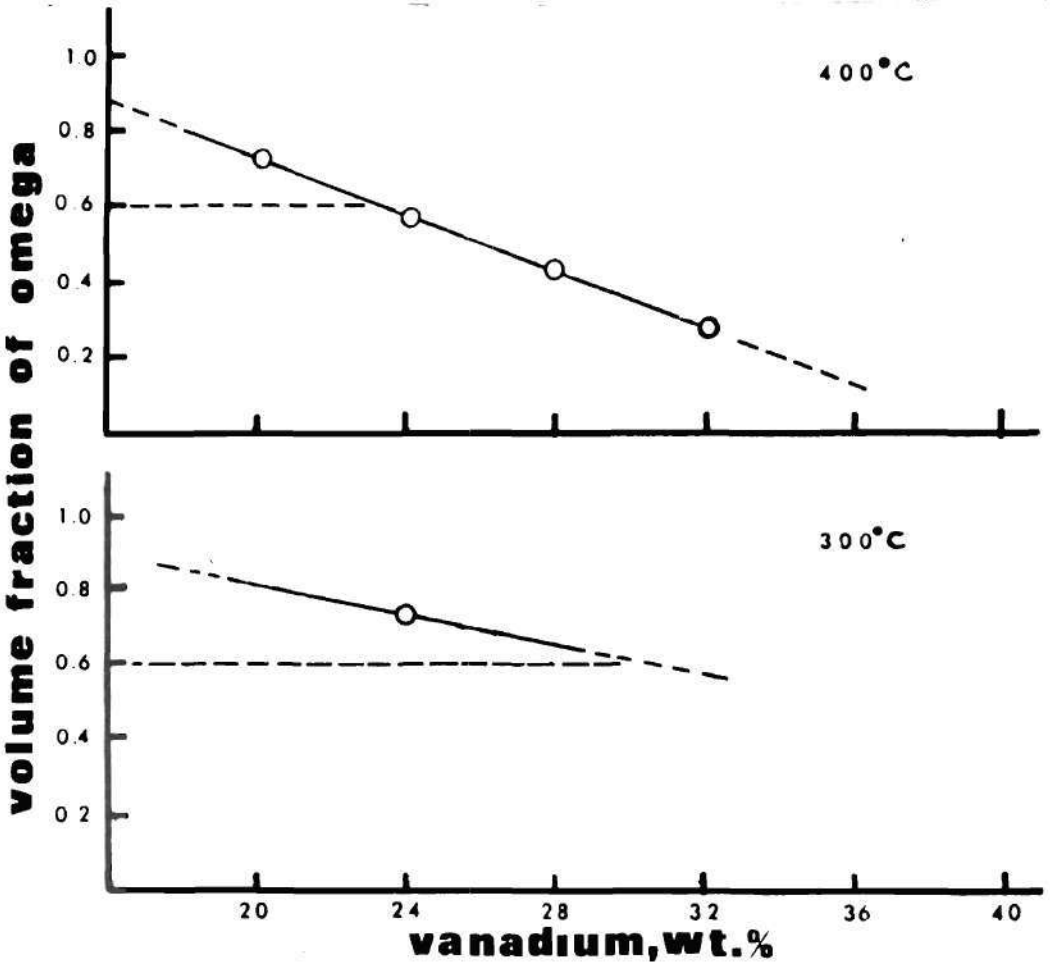

Figure 20. The Variation of Omega Volume Fraction with Composition in Some Ti-V Alloys

occurs. Associated with this transition from twinning to slip is a marked reduction in overall ductility.

This relationship of the omega volume fraction to observed deformation behavior can be seen clearly from a consideration of the elementary phase relations between the omega and beta phases. By comparing the compositions and deformation behavior listed in Table 2 with the three points in Figure 1 labeled "a", "b", and "c", the relationship is illustrated. The three points respectively correspond to thermal treatments and compositions of

the Ti-20% V aged 10 minutes at 400°C, and the Ti-24% V alloy aged one hour at 400°C and eleven hours at 300°C. Treatments "a" and "c" result in an embrittled alloy deforming by slip while treatment "b" results in a ductile alloy deforming by twinning. It is clear that a decrease in aging temperature will promote ductile behavior by reducing the maximum attainable omega volume fraction. Greater strengths can be obtained at the expense of alloy ductility by elevating the aging temperature during isochronal aging. Alternatively, under isothermal aging conditions, an increase in the solute content reduces the amount of omega present after aging and enhances alloy ductility. A decrease in solute content under isothermal aging conditions can promote a transition from ductile to brittle behavior with accompanying higher strengths.

The determination of the role of omega in effecting such marked changes in deformation behavior is facilitated by the use of TEM methods of microstructural analysis. SAD patterns carefully taken within the coarse twins of the Ti-24% V alloy indicate all four orientation variants of the omega are present within the coarse twins. In the Ti-28% V alloy, the evidence suggests no more than one omega orientation variant but probably none exists within the twins.

A consideration of the consequence of passage of an a/6<111> shear in a beta plus omega microstructure facilitates the understanding of this surprising result. There are several possible phenomenological consequences of the passage of a twin shear through the omega structure: i) the omega particles may be unsheared and bypassed by the twinning dislocations, ii) the omega may be sheared along with the beta into a twinned relationship, iii) the omega particles may be reverted by the

twin shear, and iv) the omega particles may be reoriented into a twinned relationship to the matrix by elastically accommodating the shear displacement during the twinning transformation. The first possibility would create singular effects within the SAD patterns taken wholly within the twins. Such SAD patterns would not exhibit omega reflections in the proper positions relative to the twinned BCC volume. If one eliminates the matrix reflections in Figure 13 and leaves the twin reflections and the omega reflections, one can see that one row of extra omega reflections would exist in the proper orientations while the other would not. In the second possibility, that the omega is reoriented by being twinned with the matrix, SAD patterns within the twin would be indistinguishable from SAD patterns within the matrix, since the crystallographic relationships would be preserved in such a process. This follows from the definition of a twin, that its structure is identical with the parent structure except for orientation. If omega is reverted by the shears (the third possibility) singular effects would also be observed in SAD patterns. There would occur only BCC reflections and twin reflections. The fourth possibility would be similar to the second, the only difference being the method in which atoms achieved their twinned positions.

As mentioned in the previous chapter, differentiation between the various possibility critically depends on analysis of SAD patterns and dark field analysis. It cannot be stressed that without careful visual examination, omega reflections may be overlooked in the background intensity of SAD patterns. A further complication is that SAD patterns reveal a maximum of two omega orientation variants whose diffraction spots are not coincident with matrix diffraction spots. Consequently, absolute

verification of the presence of all four orientation variants' requires at least one more SAD pattern containing the other two variants non-coincident reflections. The limitation on tilting in the electron microscope used in this study prevents such verification. Since omega occurs in a random distribution of orientations, the detection of two orientation variants is assumed to imply the existence of the others. Indeed, the dark field images and SAD patterns of Figures 12 and 15 support this assumption.

The TEM evidence suggests either mechanism (ii), (iii), or (iv) may explain the result that omega is preserved within the coarse twins in the Ti-24% V. To decide which of these is occurring, let us examine the beta/omega crystallography to ascertain if compatible twinning or slip modes exist in both structures.

There is no crystallographic information on potential slip or twinning deformation in the omega crystal structure. An initial idea can be obtained by considering the difference between the HCP structure and the omega hexagonal structure. The HCP structure has atoms in the omega unit cell situated at co-ordinates 0,0,0, and 1/3,2/3,1/2, while the omega structure has atoms at these positions and at 2/3,1/3,1/2. The two structures differ in that the HCP based structure has three atoms in the plane at z = 1/2, and the omega structure has six atoms in this plane. The consequence of the extra atoms is a greatly reduced c/a ratio and much less smooth crystallographic planes. The omega structure is suggested to be the metallic homologue to the graphite structure. Strong bonding within the basal planes combined with weak bonding between basal planes promotes basal slip while diminishing the probability of non-basal slip. Bearing in mind (i) nonbasal slip is preferred over basal

slip as a result of this graphite-type bonding, (ii) in the BCC structure, twinning in the $\{\overline{1}12\}$ <111> mode involves the motion of atoms in the $\{112\}$ plane of a/6 <111>, and (iii) in hexagonal structures a reduced c/a ratio favors nonbasal slip on planes $\{10\overline{1}n\}$, where n is a small integer; let us assume the planes that can serve as slip or twinning planes in omega are of similar index to those in the normal HCP structure. The omega planes that are parallel to the $\{\overline{1}12\}$ beta planes can be calculated from Appendix II. Since the <111> and $\{\overline{1}12\}$ are always parallel to omega planes and direction of similar indices, the relationship of one set of <111> directions and $\{\overline{1}12\}$ planes in beta to the parallel planes and directions in the four omega orientation variants may be generalized to the remaining <111> directions and $\{\overline{1}12\}$ planes. Table 4 lists the commonly observed HCP slip systems, while Tables 5 and 6 list the parallel omega planes and directions to the [111] and $\{\overline{1}12\}$. It can be seen from the information in these tables that two omega orientation variants possess potential parallel slip planes to the beta planes, but that only one orientation variant possesses a conceivable slip direction parallel to the <111>. In view of the discussed homologous nature of the graphite and omega structures, $\bar{c}$ slip seems unlikely to occur. In fact, these criteria suggest there exists no slip or twinning system in the omega structure compatible with the direct atomic motions involved in $\{\overline{1}12\}$ <111> twinning. Without consideration of the experimental results one would conclude that of the previously mentioned possibilities, only (i) or (iii) are active upon twinning deformation. Since the results definitely establish the existence of omega orientation variants within the twins, another mechanism that these two, not depending on specific

Table 4. The Commonly Observed Slip System in HCP Based Structures

$\{10\bar{1}0\}\ \langle 1\bar{2}10\rangle$ or $\langle \bar{1}\bar{1}23\rangle$
$\{10\bar{1}n\}\ \langle 1\bar{2}10\rangle$
$\{11\bar{2}2\}\ \langle \bar{1}\bar{1}23\rangle$
$(0001)\ \langle 1\bar{2}10\rangle$

Table 5. The Omega Planes Parallel to the (112) Beta Plane

Omega Orientation Variant			
1	2	3	4
$(0\bar{3}30)$	$(\bar{3}2\bar{1}1)$	$(\bar{1}\bar{2}31)$	$(01\bar{1}\bar{2})$

Table 6. The Omega Directions Parallel to the Beta a/6 <111>

Omega Orientation Variant			
1	2	3	4
$1/3[000\bar{1}]$	$1/9[0,32,\bar{3}\bar{2},3]$	$1/9[\bar{3}\bar{2},32,0,3]$	$1/9[0,32,\bar{3}\bar{2},3]$

one to one coordinated atom motion in the two structures must be active.

It is intuitive from the definition of a twinning shear that were each coherent omega volume constrained to move with the adjoining BCC volume in a twin process, the result of the BCC twin mirror rotation would place the omega in the same relative orientation to the twinned BCC volume as it had to the original untwinned BCC volume. The only require-

ment which would be necessary to impose is that the omega be able to withstand the intermediate lattice distortion in the twinning transformation.

There is one omega orientation variant whose orientation to the matrix and twin is such that it possesses identical crystallographic relationship in both matrix and twin, except the sense of positive displacement is reversed. Figure 21 illustrates this result. This orientation variant's $\bar{c}$ axis is the parallel to the <111> twin shear direction. This variant also is the one observed in association with the rods in Figure 14-16. A twin can approach such omega orientations and bypass them without disrupting the omega structure if the intermediate atomic motions in the twinning process can be accommodated. Such a propagation process, in which all variants except this one are destroyed could partially explain the observed results, yet it leaves unaccounted how other orientation variants within the Ti-24% V ductile alloys are preserved. It still does not explain the anomolously high twinning frequency in the low solute aged or quenched alloys.

A potential propagation mechanism in which both omega and beta finally exist in a twinned orientation in the Ti-24% V alloy can be qualitatively envisioned if the twinning process in the two phase structure is considered as a process of passage from one equilibrium (or metastable equilibrium) state to another identical state by surmounting an intermediate potential barrier to the process. This would describe the passage of a beta plus omega microstructure from the untwinned to the twinned condition. Surmounting the intermediate potential barrier would only necessitate the necessary applied stress to dilate or revert the omega lattice so the omega atoms may accommodate the $\{\bar{1}12\}$ <111> twinning

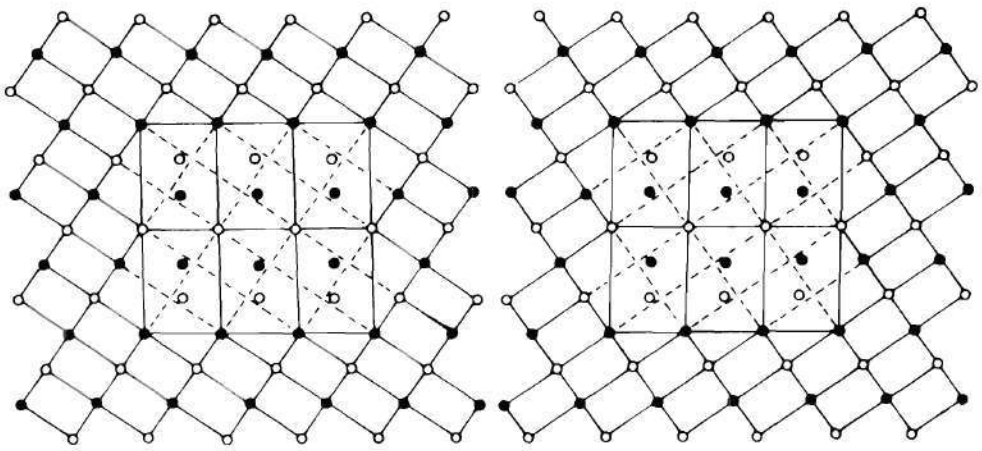

(a) (b)

Figure 21. An Illustration of the Identical Orientation to Both Twin and Matrix of the Omega Orientation Variant Whose $\bar{c}$ Axis is Parallel to the <111> Twin Shear Direction. The Crystallographic Planes and Directions are the Same as in Figure 2. a) The Untwinned Condition, b) The Twinned Condition

shear. A subsequent relaxation to the metastable equilibrium positions would restore the omega structure. A relaxation to the beta atomic sites would correspond to the total reversion of the omega structure. Figure 22 illustrates this atomic mechanism. The atoms in the prior omega have misfit bonds for either structure. By allowing atomic shuffles of $\pm$ a/12 <111> to the "square" positions, a twinned BCC structure can be obtained. By allowing atomic shuffles of $\pm$ a/6 <111> to the "X" positions, the omega structure can be reformed. The ability of the atoms to assume the beta or omega atomic sites ought to depend on the local composition of the lattice. As the lattice composition decreases the tendency for an atom to occupy the omega stacking positions relative to its neighbors exceeds the tendency to occupy the less stable, but closer beta atomic sites. It is concluded that only alloys with less than 24% V preserve the omega phase within

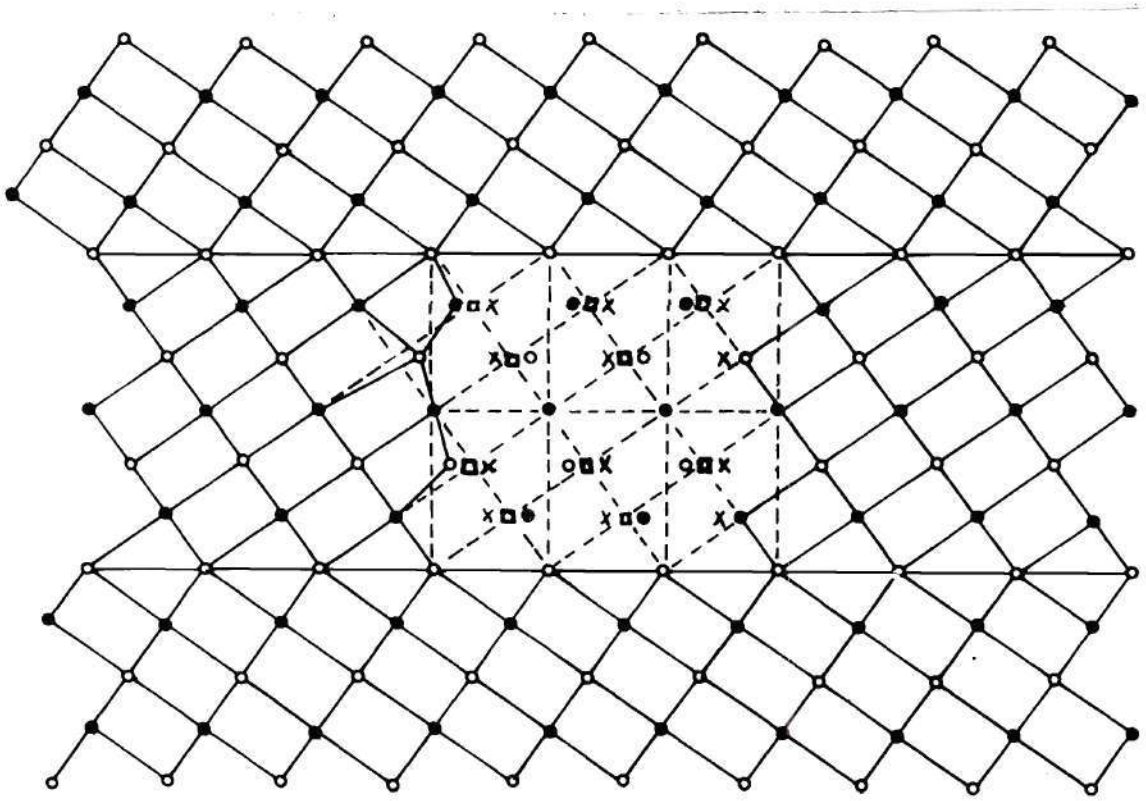

Figure 22. The Creation of a $\{\overline{1}12\}$ <111> Shear Twin in the BCC Beta Structure and Destruction or Dilation of the Omega Structured by the Progressive a/6 <111> Twin Shear. The Crystallographic Orientation is the same as Figure 2.

the coarse twins. Apparently such factors as increased solute content of the alloy and the higher initial and ultimate omega/beta misfit preclude the preservation of omega in alloys with more than 24% V.

It behooves us to examine a possible nucleation process in these alloys. It has been established that a $\{\overline{1}12\}$ <111> twin may form without a net shear or unique applies shear stress by a shuffle mechanism not unlike that proposed to explain the athermal omega transformation (24,54). Figure 2 illustrated both twin and omega shuffle transformations. Since a shuffle mechanism of this type can be operative without an applied shear regardless of the magnitude of the shuffles, a twin embryo may be created by random $\pm$ 1/12

<111> shuffles. If such a twin embryo experiences a favorably appied shear stress it ought to grow in size, twinning the cubic volume. Such a shuffle type nucleation mechanism for {112} <111> twinning ought to be active in these alloys; especially if the twin can arise as a result of atomic displacements on half the normally expected displacements and can deform the lattice with less net loss of omega than the slip process.

It is known that the a/12 <111> row displacements are stable features of certain solute content zirconium and titanium beta lattices. If such row displacements occur at a properly oriented omega/beta interface, even if only the result of random atomic fluctuations, a surprising result occurs. A small twinned beta lattice is created in the previous omega particle while the adjoining beta lattice experiencing the same shuffles is transformed to the previously existing orientation of the omega phase. In the presence of an applied stress, the twinned volume can grow and propagate a $\{\overline{112}\}$ <111> deformation twin. Figure 23 illustrates how the nucleation may occur and subsequently propagate. This mechanism is based on the hypothesis that the coherent relationship between the two lattices will encourage atomic motions in the interface to be accommodated in both structures. The shuffles in Figure 23 can result in no net loss of omega while allowing alloy deformation by twinning. Although the applied stress cannot effect such shuffles, once they occur in a volume of critical size, the twinned BCC structure ought to grow. The experimental observation of a row morphology of twin nuclei associated with single orientation variants of omega support such a result.

The effects of such shuffles and the possibility of their occurrence obviously depend on the alloy solute content. One would expect this

(a)

(b)

(c)

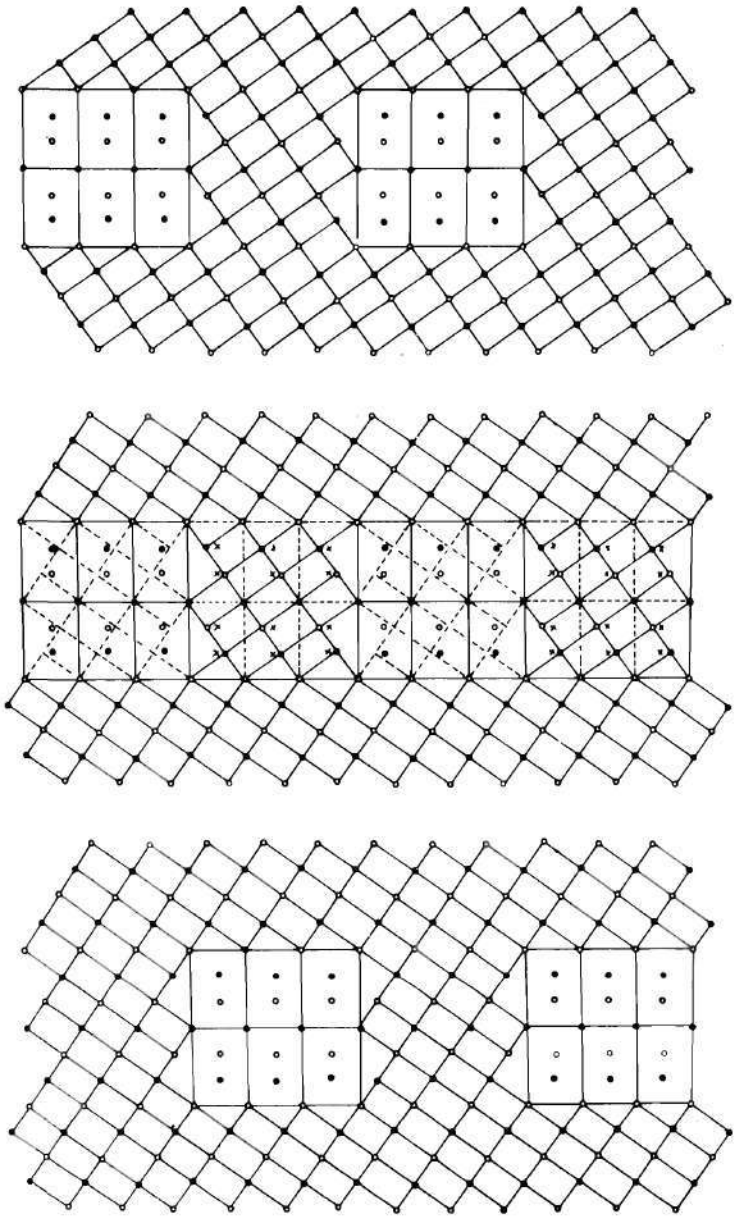

Figure 23. The Nucleation and Propagation of a $\{\overline{1}\overline{1}2\}$ <111> Deformation Twin at a Properly Oriented Row of Single Orientation Variant Omega Particles. a) The Untwinned Lattice, b) The Nucleation of a $\{\overline{1}\overline{1}2\}$ <111> Twin by $\pm$ 1/12 <111> Shuffles in the Beta: Omega Interface, c) The Subsequent Propagation of the Twin. Note The Omega Particles can be Destroyed and New Particles Created in the Adjoining Lattice. The Crystallographic Orientation is that of Figure 2.

nucleation mechanism to occur in a BCC structure in which the 1/12 <111> atomic displacements are a stable feature of the lattice. This would correspond to the compositional range in which omega can be produced athermally or by isothermal aging. In the approximate range of occurrence of athermally produced omega one would expect no reversion or loss of omega as the shuffles can easily reoccur after twinning as they did previous to twinning. It is likely that in alloys of higher composition such a process would be accompanied by the spontaneous reversion of the omega atoms to the closer BCC sites. This is a result of the fact that the athermal transformation to omega diminishes with increasing solute content. The closest BCC positions are twin related to the matrix structure. It is believed the latter situation occurs in the experimental alloys with greater than 24% vanadium, while the former occurs in alloys with less solute content.

In view of these facts, a formal process of nucleation and propagation of $\{\bar{1}12\}$ <111> twins in the Ti-V omega plus beta microstructure can be proposed. A $\{\bar{1}12\}$ <111> twin embryo can be nucleated by random correlation of $\pm$ a/12 <111> row displacements in the vicinity of an omega/beta interface whose omega $\bar{c}$ axis is parallel to the resulting <111> twin shear. In alloys which spontaneously transform to the omega structure, i.e., alloys with less than about 24% V, if these atomic shuffles occur in a one to one correspondence across the beta/omega interface, no net loss of omega need occur upon twin nucleation. In other omega bearing alloys, i.e., alloys with greater than 24% V, the omega is expected to totally revert to the BCC twin or matrix sites in the nucleation process. Thus alloys may nucleate a twin by stable $\pm$ a/12 <111> atomic displacements

when the matrix solute content is below 24% V. With aging, or at higher solute contents, the matrix is enriched in solute and the $\pm$ a/12 <111> displacements decrease in probability and twinning can be expected to diminish in frequence and/or the necessary local stress for nucleation of twinning to increase. Twin nucleation in these alloys (with matrix composition greater than 24% V) ought to occur by reversion of the omega to twin BCC positions. A reverted omega particle whose new BCC structure is favorably oriented to the applied shear stress ought to increase in size and twin the cubic volume as discussed in relation to lower solute alloys. Thus, long aging in which matrix solute content increases without the omega volume fraction exceeding 0.6, ought to produce an alloy which behaves similarly to an alloy which had a greater initial solute content.

In the propagation of the twins, the encounter of other omega orientation variants of the same crystallographic nature by twin shears will not impede their propagation since these orientation have the same orientation in and outside the $\{\overline{1}\overline{1}2\}$ <111> twin. This orientation can be preserved directly by considering the twin propagation process as passage from one equilibrium state to another identical state by surmounting an intermediate potential barrier represented by the intermediate positions of omega atoms in Figure 22. Since these positions are not equilibrium sites but represent a state of distorted bonding for both structures, a driving force to reoccupy either the cubic or omega sites will exist. The site occupied depends on the solute content, as low solute contents (less than 24% V) stablize omega and higher solute contents stablize the beta structure. Even though the treatment used to arrive at this nucleation and propagation mechanism utilized only consideration of the effect of

twin shears on one variant of omega, atoms in other orientations will be displaced from equilibrium sites in twin propagation by the same magnitude. They will experience similar driving forces to readopt either BCC or omega atomic sites. A test of the ease of twin nucleation and propagation, as well as the ability of the reverted omega to retransform could be determined by aging a Ti-24 and Ti-28% V alloy for extended time at 300°C to produce a moderate omega volume fraction with a great compositional difference between the matrix and omega. The twin nucleation in a matrix of large solute content and the ability of a low solute content reverted omega region to retransform to omega after twinning could be determined and conclusions generally applied to other alloy compositions.

This model predicts $\{\overline{1}12\}$ <111> twinning to occur in all alloys containing the omega phase, although omega is not expected to be preserved unless the gross solute content is below about 24%, or the omega particles have reduced their solute content to this value or lower. Even though nucleation may not be enhanced at higher solute contents where the $\pm$ a/12 <111> omega transformation needs a thermal assist, omega is expected to be preserved on twinning after aging has lowered the omega solute content to the range of 24% V or lower. Although the omega may be reverted by the twin shears, as by slip, the twin shears in the omega uniformly shear the particles and matrix, not heterogeneously destroying the omega to create an easier path for slip. This may be why the omega containing alloys which twin have such good ductility relative to those which deform by slip; that a normally considered macroscopically heterogeneous deformation mechanism like twinning allows the matrix and precipitate to be uniformly sheared creating less probability of stress concentrations

which may result in local lattice breakdown and crack initiation.

Features observed in the substructure by TEM in the ductile alloys support the existence of this proposed twinning mechanism. The rod features observed in Figure 12-16 clearly are the sites of origin of the $\{\bar{1}12\}$ <111> twinning. DF analysis shows that one omega orientation variant, whose $\bar{c}$ axis is parallel with the <111> twin shear direction, is associated with these rods. The rods are also parallel to the twin shear direction and appear composed of the omega particles. Figures 17 and 18 as well as the optical microscopy, show that the coarse twins are created by repeated layering of the microtwins. In the Ti-24% V alloy, Figure 12 shows that multiple orientations of omega exist within the coarse twins, an experimental fact which virtually necessitates an athermal transformation of the disrupted omega lattice back to omega as suggested in Figure 22. At higher solute contents, SAD ($\gtrsim$ 24% V) analysis suggests none or one omega orientation variants are preserved after twinning. Both situations can be accounted for by the proposed mechanism since the tendency to form omega depends on solute content and the possibility the existing variant is oriented properly in both twin and matrix. At higher solute contents it is noted that coarse twinning does not occur in the as quenched condition, but does occur in the aged condition. This suggests some lower fraction of omega is necessary for twinning. It is also noted that even in the embrittled alloys the twinning has not been eliminated, but only relegated to a secondary role in macroscopic deformation.

As the volume fraction of the omega phase becomes greater in the aged alloys, or low solute quenched alloys, other factors may come into

predominance which can alter the macroscopic alloy deformation behavior. The influence of each phase on the macroscopic deformation can be considered as arising from the relative volume of each in which its deformation mechanisms are operative. In alloys containing only a small amount of a second phase, one expects the major contribution to alloy deformation to arise from the predominant phase. This, of course, discounts singular effects such as unusual phase distribution, e.g., grain boundary precipitates. Deviations from pure metal deformation behavior result from the influence of a second phase on the primary phase's deformation. An alloy containing a larger fraction of ductile primary phase than secondary brittle phase will possess some ductility as long as cracking is limited to the smaller volume of second phase. As the second phase's volume fraction increases, its influence on macroscopic deformation ought to wax while the other phase's influence diminishes. When the secondary phase becomes the predominant phase, the earlier primary phase can no longer impose necessary constraints arising from its deformation behavior. If the second phase is nondeformable and brittle, the alloy behavior ought to approach this behavior.

In the present case one must consider the fact that the twinning is a homogeneous deformation mechanism, each plane in the twinned volume being sheared. Every {112} plane in the volume experiences a shear or shuffle, deforming the omega phase in a uniform manner. As greater volume fraction of omega occurs, a decreasing fraction of cubic material must store the necessary energy for dilation of the majority omega phase in order for a large scale dilation/twin/retransformation mechanism to be operative. This means a greater local stress within the cubic volume

must exist to exert the same dilational energy per particle in the larger omega volume fraction. At some point the softer matrix begins to yield locally before a large enough stress can be attained to effect twinning. The result is an embrittled alloy. A Ti-24% V alloy with 0.7 omega volume fraction must store more than twice the energy in less than one half the cubic volume that exists in the ductile alloy in order to effect the same twinning dilational force per particle. It is clear that as one reduces the fraction of beta, the required energy density in beta to effect the same twinning process demands a greater local stress. In attempting to store the necessary energy for twinning, the beta can deform heterogeneously by slip. If reversion occurs at any site within the lattice as a result of slip, a much easier path of deformation has been created. Concommitant slip band formation and the build up of stress concentrations within them will rapidly lead to crack initiation and macroscopically brittle failure. Such a process is consistent with the observed substructure of the embrittled alloys (Figure 13).

This point concerning the relative influence of each phase can be put into terms related to the omega volume fraction to show the qualitative way each phase's influence on macroscopic deformation varies. It is not maintained the behavior of the following expression accurately describes the exact influence of each phase, but indicates the direction of change of influence of each phase with its volume fraction. Let the relative influence of the beta deformation modes to the influence of the omega deformation modes on macroscopic deformation be noted R_β. Define R_β as follows:

$$R_\beta = \frac{G_b}{G_w} \text{ (volume of beta per omega particle)}$$

$$= \frac{\text{(volume of beta per unit alloy volume)}(G_b)/(G_w)}{\text{(volume of omega per unit alloy volume)/(volume of one omega particle)}}$$

$$= \frac{G_b\ f_b\ (d_w)^3}{G_w\ f_w}$$

where f_b, f_w, G_b, G_w, and d_w are the volume fraction of beta and omega, the shear modulus of beta and omega, and the omega particle edge length, respectively. It is obvious that when f_b exceeds f_w the matrix influence can be greater than the precipitate's influence. It is likely the values of the shear modulus could affect the exact value at which a transition occurs, but the beta cannot exert a greater influence than the omega for omega volume fractions much in excess of 0.5. Since the beta is interconnected, while the omega exists isolated particles, the influence of beta on macroscopic deformation could persist after f_b falls below 0.5. This is in agreement with the result that omega volume fractions of 0.6 to 0.7 are needed to effect a transition from ductile to brittle behavior. The fact that twinning does not suddenly cease, but continues on a diminished scale even when the predominant macroscopic deformation behavior is embrittled failure by slip, supports this conception of omega's influence on alloy ductility.

CHAPTER VI

CONCLUSIONS

1. Deformation of Ti-V alloys within the compositional range of 20-40% vanadium containing less than 0.6 volume fraction omega occurs predominantly by coarse $\{\overline{1}12\}$ <111> twinning.

2. In similar solute content alloys possessing greater than 0.6 volume fraction omega, deformation occurs predominantly by planar slip.

3. The presence of the omega appears necessary for the coarse twinning to occur.

4. Marked ductility is exhibited by those omega bearing alloys whose predominant deformation mode is coarse twinning, while those alloys whose predominant deformation occurs by slip are markedly embrittled.

5. Failure of the embrittled alloys appears to occur by crack initiation in the slip bands.

6. The omega phase is not destroyed by the twinning transformation in as quenched or aged alloys whose vanadium content is less than about 24%, while in others of higher solute content it is destroyed, either totally or partially.

7. Deformation twinning occurs similarly in alloys that contain either athermally produced or isothermally produced omega phase, although in alloys whose net solute content or omega solute content exceeds about 24% V the omega phase does not appear to be preserved.

8. The corase $\{\overline{1}12\}$ <111> twinning occurs by repeated microtwinning on parallel {112} planes, homogeneously establishing a large twinned volume.

9. The ductile behavior of alloys with less than 0.6 volume fraction omega is suggested to result from the induced deformation twinning. Twinning, normally considered a less ductile and more heterogeneous deformation process than slip, produces ductile behavior as a result of the microscopically homogeneous nature of the planar twin shears. Slip results in a microscopially heterogeneous shearing of the omega in which easier paths for subsequent slip deformation are created by reverting the omega locally.

10. The transition from ductile to brittle behavior can be qualitatively understood by considering the variation of relative volume of beta per omega particle available for storing energy for the athermal dilation or reversion of the omega in the intermediate step of the twinning transformation.

11. A mechanism is proposed which explains both the nucleation and propagation of twins in duplex beta omega microstructure. Nucleation is hypothesized to occur by $\pm$ a/12 <111> shuffles at the interface of a properly oriented omega orientation variants precipitate and the beta matrix. Subsequent propagation occurs by the expansion of the twinned volume under the influence of an applied shear stress. The preservation of omega in certain compositions is consistent with the proposed mechanism.

APPENDIX I

THE HEXAGONAL BASIS

In structures of hexagonal symmetry, several choices of crystallographic basis exist. Of the three encountered most commonly, the rhombohedral, orthorhombic and hexagonal, only the latter two are used extensively in the metallurgical literature. In the orthorhombic basis and the hexagonal basis which utilized three axes ($\alpha = 120^\circ$, $\beta = \gamma = 90^\circ$) and three indices, geometrically similar planes and directions do not possess similar indices except in special cases. The hexagonal basis utilizing four axes; three spaced 120° apart and one perpendicular to the other three, does not possess the mathematical simplicity of orthogonal coordinate systems; however, the axes coincide with the natural cyrstallographic symmetry of the structure. Similar planes and directions possess similar indices in the four axes system.

In order to shorten the notation of the four index basis, the third index is often omitted and its presence noted explicitly by the positioning of a period in its place, e.g., (hk.l). This may cause ambiguity since without the period the indexing is confused with the three axes hexagonal system. This method of indexing planes and directions according to the four axes basis is seen in two forms. One is called the four axes, four index basis, the other the four axes, three index basis. Indices of planes (reciprocal lattice directions) may be compared between these two by omitting the third redundant index. Real lattice directions may not be compared directly between these two bases as the reciprocal

lattice basis used in the four index basis is not reciprocal to the corresponding direct lattice basis. In order to simplify the crystallographic formula and to maintain a relatively unambiguous index system that is readily compared to the cubic basis, the notation of Otte and Crocker is used (58,59). The three index, three axes hexagonal basis or the orthorhombic basis is used in calculations, sacrificing the similarity of indices of similar planes and directions for mathematical simplicity. Whether referring to planes or directions the three axes basis is called the Miller-Bravais indices are used where comparison to existing work is facilitated by their use. The use of the hexagonal notation, as well as errors in common metallurgical texts are discussed in the cited references (60,61).

APPENDIX II

THE CRYSTALLOGRAPHY OF THE FOUR OMEGA ORIENTATION VARIANTS

The omega phase is a hexagonal or trigonal structure depending on its solute content. The three atoms in the unit cell are at positions 000, 1/3,2/3,1/2 and 2/3,1/2,1/2 in the hexagonal structure. The specific symmetry, trigonal or hexagonal, depends on the position of atoms within the atomic plane at z = 1/2. When the atoms are totally confined in the plane it is hexagonal, otherwise (at higher solute contents) it is trigonal.

If the beta structure is represented by the same unit cell as the omega, the cubic atoms are at 000, 2/3,1/3,1/3 and 1/3,2/3,1/3. If the latter two atoms are translated by $\pm$ 1/12 <111>, the omega structure results (55). Such a transformation results in four distinct omega orientations, each with the $\bar{c}$ axis parallel to a $\langle 111 \rangle_\beta$ direction. The orientation relationship is:

$$\{0001\}_\omega \;//\; \{111\}_\beta \text{ and } \langle 1\bar{1}0 \rangle_\beta \;//\; \langle 11\bar{2}0 \rangle_\omega \; .$$

Utilizing this relationship, the four variants' bases to the cubic basis may be obtained. These bases may be used to construct simple transformation matrices relating cubic planes and directions to hexagonal planes and directions. These relationships between the two bases are listed in Table 7.

Table 7. The Direct and Reciprocal Lattice Basis of the Omega Orientation Variants Relative to the Cubic Beta Lattice Basis

	Omega Orientation Variant			
	1	2	3	4
$\bar{a}_{\omega n}$ (B)	$1/2[\bar{2}20]$	$1/2[0\bar{2}2]$	$1/2[0\bar{2}\bar{2}]$	$1/2[\bar{2}20]$
$\bar{b}_{\omega n}$ (B)	$1/2[20\bar{2}]$	$1/2[220]$	$1/2[220]$	$1/2[202]$
$c_{\omega n}$ (B)	$1/2[\bar{1}\bar{1}\bar{1}]$	$1/2[\bar{1}11]$	$1/2[1\bar{1}1]$	$1/2[11\bar{1}]$
$\bar{a}^*_{\omega n}(B)^t$	$1/3[\bar{1}2\bar{1}]$	$1/3[1\bar{1}2]$	$1/3[121]$	$1/3[\bar{1}21]$
$\bar{b}^*_{\omega n}(B)^t$	$1/3[11\bar{2}]$	$1/3[211]$	$1/3[21\bar{1}]$	$1/3[112]$
$\bar{c}^*_{\omega n}(B)^t$	$1/3[\bar{2}\bar{2}\bar{2}]$	$1/3[\bar{2}22]$	$1/3[2\bar{2}2]$	$1/3[22\bar{2}]$

To obtain the indices of an omega plane parallel to an arbitrary beta plane, $[h'k'l']^{*t}$, one utilizes the following relations:

$$\begin{bmatrix} \bar{a}_{\omega n} \ (B) \\ \bar{b}_{\omega n} \ (B) \\ \bar{c}_{\omega n} \ (B) \end{bmatrix} \begin{bmatrix} h' \\ k' \\ l' \end{bmatrix}_{\beta} = \begin{bmatrix} h \\ k \\ l \end{bmatrix}_{\omega n}$$

The inverse operations may be accomplished by determination of the reciprocal basis of omega relative to the beta reciprocal basis. That is:

$$[u'v'w']_{\beta} \ [\bar{a}^*_{\omega n} \ (B)^t, \ \bar{b}^*_{\omega n} \ (B)^t, \ \bar{c}^*_{\omega n} \ (B)^t] = [uvw]_{\omega n}$$

and:

$$[\bar{a}^*_{\omega n} \ (B)^t, \ \bar{b}^*_{\omega n} \ (B)^t, \ \bar{c}^*_{\omega n} \ (B)^t] \begin{bmatrix} h \\ k \\ l \end{bmatrix}_{\omega n} = \begin{bmatrix} h' \\ k' \\ l' \end{bmatrix}_{\beta}$$

The normal direction, [defg], to an omega plane (hkiℓ) is given by the relation:

$$[defg] = [h,k,i,(c/a)^2\ell] \quad (61).$$

For the omega structure, $c/a \sim \sqrt{6}/4$; therefore:

$$[defg] = [h,k,i,\ 3/8\ \ell].$$

BIBLIOGRAPHY

1. J.C. Williams, Proceedings of the Second International Conference on Titanium, M.I.T., Titanium Science and Technology, Jaffee and Burte, ed., Plenum Press, N.Y. (1973) 1433.

2. M.J. Blackburn and J.A. Feeney, J. Inst. Met., 99 (1971) 132.

3. S.L. Sass and B. Borie, ONR Technical Report No. 7, Contract N0014-67-A-0077-0012 (1973).

4. F.W. Ling, E.A. Starke Jr., and B.G. Lefevre, Met. Trans. (1973) 179.

5. S. Mahajan and D.F. Williams, International Metallurgical Reviews, 18 (1973) 43.

6. R.W. Cahn, Advances in Physics, 3 (1954) 363.

7. D. Hull, Fracture of Solids, Interscience, New York (1963) p. 43 ff.

8. J.W. Christian, The Theory of Transformations In Metals and Alloys, Pergamon Press, Oxford (1965).

9. E.O. Hall, Twinning and Diffusionless Transformations in Metals, Butterworths, London (1954).

10. R.W. Cahn, Nuovo Cimento (Suppl.), 10 (1953) 350.

11. M.K. Koul and F. Breedis, Acta Met. (1970) 579.

12. B.S. Hickman, TAIME, vol. 245 (1969) 1329.

13. M.J. Blackburn and J.C. Williams, TAIME, 242 (1968) 2461.

14. B.S. Hickman, J. Mat. Sci., 4 (1969) 554.

15. J.C. Williams, Titanium Science and Technology, vol. III (1973) 1433.

16. S.L. Sass, Acta Met. 17 (1969) 813.

17. J.C. Williams, N.E. Paton, and G.P. Rausch, unpublished research (1972).

18. J.C. Williams, D. deFontaine, and N.E. Paton, Met. Trans. 4, (1973) 2701.

19. J.M. Silcock, Acta Met. 6 (1958) 481.

20. I.A. Bagariatskii, et al., Dolk Akad. SSR, 105 (1958) 1225.

21. B.S. Hickman, J. Institute Met., 96 (1968) 330.

22. J.C. Williams and M.J. Blackburn, Trans. AIME, 245 (1969) 2352.

23. W.G. Burgers, Physica's Grav., 1 (1934) 109, 561.

24. B.A. Hatt and J.A. Roberts, Acta Met. 8 (1960) 575.

25. J.M. Silcock, Acta Met. 7 (1959) 359.

26. B.A. Bilby and A G. Crocker, Proc. Roy. Soc. A, 288 (1965) 240.

27. M. Bevis and A.G. Crocker, ibid, 304 (1968) 123.

28. M. Bevis and A.G. Crocker, ibid, 313 (1969) 509.

29. R.W. Cahn, Deformation Twinning, Gordon and Breech, New York (1964).

30. H. Kiho, J. Phy. Soc. Japan, 9 (1954) 739.

31. H. Kiho, ibid, 13 (1958) 269.

32. D.M.M. Guyncourt and A.G. Crocker, Acta Met. 18 (1970) 805.

33. J O. Steigler and C.J. McHargue, Deformation Twinning, Gordon and Breech, New York (1964) p. 209.

34. Ibid, page 77.

35. J.S. Chun and J.G. Byrne, Phil. Mag, 20 (1969) 291.

36. M.J Blackburn and J A. Feeney, J. Inst. Met., 99 (1971) 132.

37. K. Ono, L.A. Rosales, S. Motokura, and A.W Sommer, Mechanical Behavior of Materials, vol. 1, published by the Society of Materials Science, Japan, Yoshida Izumidono-cho, Sakyo-Ku, Kytoto 606, Japan, Maeda Shink-do Printing Co., LTD, Japan (1972) p. 66.

38. M.A. Jaswon and D.B. Dove, Acta Cryst, 9 (1956) 621.

39. M A. Jaswon and D.B Dove, ibid, 10 (1957) 14.

40. M.A. Jaswon and D B. Dove, ibid, 13 (1960) 232.

41. ASTM Standards, part 31, published by the American Society for the Testing of Materials, Philadelphia (1970) pp. 203-207.

42. M.J. Blackburn and J.C. Williams, TAIME, 239 (1967) 287.

43. P.B. Hirsch, A. Howie, R.B. Nicholson, D.W. Pashley, and M.J. Whelan, Electron Microscopy of Thin Crystals, Butterworths, London (1965).

44. L.E. Murr, Electron Optical Applications in Materials Science, McGraw-Hill Co., New York (1970).

45. G. Thomas, Transmission Electron Microscopy of Metals, John Wiley and Sons, New York (1962).

46. E. Orowan, Dislocations in Metals, published by the AIME, New York (1954) p. 116.

47. A.H. Cotrell and B A. Bilby, Phil. Mag., 42 (1951) 573.

48. A.W. Sleeswyk, Acta. Met. 10 (1962) 705.

49. A.W. Sleeswyk, ibid, 8 (1963) 1467.

50. K. Ogawa, Phil. Mag., 11 (1965) 217.

51. R. Priestner and W.C Leslie, Phil. Mag., 11 (1965) 895.

52. A.T. Balcerzak and S.L. Sass, Met. Trans., 3 (1972) 1601.

53. Didier deFontaine and Ryochi Kikuchi, Acta Met. 22 (1974) 1139.

54. M F. Ashby, Phil. Mag., 21 (1970) 399.

55. S.L. Sass, The Structure and Decomposition of Titanium and Zirconium BCC Solids Solutions, ONR Technical Report No. 12, Contract N000 14-67-A-0077-0012.

56. R.J. Wasilewski, Met. Trans., 1 (1970) 2641.

57. R.J. Wasilowski, Met. Trans., 6A (1975) 1405.

58. H.M. Otte and A.G. Crocker, Phys. Stat. Sol., 9 (1965) 441.

59. Ibid, 9 (1966) K25.

60. P.G. Partridge and R.W. Gardiner, Acta Met., 15 (1967) 387.

61. C R Rarey, J. Stringer, and J.W. Edington, Trans. AIME, 236 (1966) 811.

62. S.L. Sass, The Stress-Induced Omega Phase Transformation in Ti-V Alloys, ONR Technical Report No. 11, Contract N00014-67-A-0077-0012 (1974).

VITA

Henry Grady Paris was born in Akron, Ohio on September 2, 1947. He graduated from the Darlington School in Rome, Georgia in 1965. In 1970 he received the degree, Bachelor of Science in Physics, co-operative plan, at Georgia Institute of Technology in Atlanta. He continued his studies in the Metallurgy program of the School of Chemical Engineering at Georgia Tech where he was elected President of the Graduate Student Body (1972-73) and received the degree, Master of Science in Metallurgy in May, 1973. He was elected to the Executive Committee of the Fulton County Democratic Party by the Democratic voters of the 27th House District and also inducted into Georgia Tech's highest student homorary, ANAK, in 1974. As a result of his work as a co-operative plan student at Oak Ridge National Laboratory in the Metals and Ceramics Division with Dr. R.W. Carpenter, he co-authored a note, "Preparation of Rhenium for Transmission Electron Microscopy", Journal of Applied Physics, vol. 39, 5809 (1968). As a graduate student in Metallurgy he co-authored the papers; "Deformation Twinning in Ordered CuPt", Materials Research Bulletin, vol. 7, 1109 (1972); "Order Hardening in Equiatomic CuPt", Metallurgical Transactions, vol. 4, 833 (1972); "The Mechanical Behavior of Quenched and Aged Beta Isomorphous Titanium-Vanadium Alloys", presented at the MATCOM Conference and Materials Science Symposium in Detroit, 1974, and "The Deformation Behavior of Quenched and Aged Beta Titanium Alloys", to be published in Metallurgical Transactions, 1975.